Pseudogap, charge order, and pairing density wave at the hot spots in cuprate superconductors

C. Pépin, V. S. de Carvalho, T. Kloss, X. Montiel

HAL Id: cea-01060904
https://cea.hal.science/cea-01060904

Pseudogap, charge order, and pairing density wave at the hot spots in cuprate superconductors

C. Pépin,[1] V. S. de Carvalho,[1,2] T. Kloss,[3,*] and X. Montiel[3]

[1]*IPhT, L'Orme des Merisiers, CEA–Saclay, 91191 Gif-sur-Yvette, France*
[2]*Instituto de Física, Universidade Federal de Goiás, 74001-970 Goiânia, GO, Brazil*
[3]*International Institute of Physics, UFRN, Avenida Odilon Gomes de Lima 1722, 59078-400 Natal, Brazil*

We address the timely issue of the presence of charge ordering at the hot spots in the pseudogap phase of cuprate superconductors in the context of an emergent SU(2) symmetry which relates the charge and pairing sectors. Performing the Hubbard-Stratonovich decoupling such that the free energy stays always real and physically meaningful, we exhibit three solutions of the spin-fermion model at hot spots. A careful examination of their stability and free energy shows that, at low temperatures, the system tends towards the coexistence of a charge density wave (CDW) and the composite order parameter made up of the diagonal quadrupolar density wave and pairing fluctuations of K. B. Efetov *et al.* [Nat. Phys. **9**, 442 (2013)]. The CDW is sensitive to the shape of the Fermi surface, in contrast to the diagonal quadrupolar order, which is immune to it. SU(2) symmetry within the pseudogap phase also applies to the CDW state, which therefore admits a pairing density *p*-wave counterpart breaking time-reversal symmetry.

I. INTRODUCTION

The discovery of charge order [charge density wave (CDW)] in the pseudogap (PG) phase in non-La-based cuprate superconductors has received steadily growing interest in recent years. Initially observed by STM in Bi2212 [1] and later in Bi2201 [2–8], the CDW phase was also observed in YBCO by quantum oscillation [9–13]. NMR [14–16] and sound experiments [17,18] confirmed the presence of a CDW phase in YBCO, while x-ray bulk spectroscopy [19–25] has clearly characterized its checkerboard ordering with a wave vector along the *x* and *y* axes $Q_x = Q_y = 0.33$ [26,27]. Deeper analysis concluded that the CDW ordering wave vector is located at the tips of the Fermi surface in the vicinity of the hot spots [25,28,29].

An additional phase transition to a checkerboard CDW ordered phase is observed at T_{CDW} [30] below the PG line at $T^\star$ [31,32], $T_{\text{CDW}} < T^\star$. Note that $T^\star$ coincides with the observation of a loop current detected by a neutron [33–37]. In the temperature-doping phase diagram, the T_{CDW} line has the typical form of a dome [38] and its magnitude is compound dependent [28,29,39,40], whereas the PG line is rather universal [39].

One of the most difficult challenges in the field is to understand how the recently observed CDW order interferes with antiferromagnetic (AFM) fluctuations and whether or not it participates in the formation of the PG phase. Although some alternative scenarios involving stronger Coulomb interactions have been considered [41–46], the proximity of the CDW ordering wave vector to the hot spots is a strong incentive to consider the spin-fermion theory, which produced the most singular behavior at hot spots [47–49]. We follow this route here, keeping in mind that the spin-fermion model has been the subject of intense recent scrutiny [48,50–57].

In the last year, it has become an increasing challenge to the community to explain how to get an emergent CDW

with the right orientation of the wave vector. Indeed, when simple random phase approximations are performed in this system, actually in either the charge or the spin channel, a maximum of intensity is obtained at the $Q = (\mathbf{Q_x}, \mathbf{Q_y})$ wave vector located on the diagonal, while no peak is experimentally observed in this direction. Some attempts to address this question have considered that a preformed PG state consisting of short-range AFM fluctuations or of a spin liquid does gap out the antinodal part of the Fermi surface, leaving behind some Fermi arcs [46,58]. In the context of the three-band model, when the hopping to Cu 4*s* orbitals is included, it is possible to rotate the wave vectors of the random phase approximation charge susceptibility to align them with the crystalline axes. The ordering wave vectors are situated at the "tip of the Fermi arc." These models suffer, however, from the consideration that whereas the "tip of the arcs" moves with temperature, the observed ordering wave vector of the modulation is nondispersing [6]. Another approach very similar to the one presented here considers directly the bare electron Fermi surface for these models and considers that a CDW with the correct wave vector can be the low-temperature order of a preformed bound state breaking time-reversal symmetry [54].

In this paper we stay in the broad context of emergent symmetries, where the *d*-wave superconductivity (SC) state of high-temperature superconductors rotates to other symmetry sectors. The underlying idea is the old idea of degeneracy of energy levels in quantum physics. When two energy levels are degenerate, it can be accidental, but it can also signal that the two energy levels are related by a common symmetry. This notion of emergent symmetry has been used in the past for cuprates with the SO(5) theory relating *d*-wave SC to the magnetic sector [59,60]. The SU(2) group was used as well in relating the *d*-wave SC to the π-flux phases, within gauge theoretic treatment of the *t-J* model [61]. Here we use the same SU(2) symmetry group, rotating the *d*-wave SC order to the charge sector. In Refs. [51,52], and [62], this symmetry has been shown to be present in the eight-hot-spot (EHS) model, where the Fermi velocity is linearized at the hot spots. In Ref. [52], a PG state was identified as the primary instability

_____
*kloss@itp.uni-frankfurt.de

of the AFM quantum critical point (QCP) within this model. In particular, it has been shown that the underlying SU(2) rotation produces a composite order parameter with a quadrupolar density wave (QDW) component in the charge sector and preformed pairs in the SC sector (QDW/SC). This short-range order is a good candidate for the PG gap phase since it breaks translational symmetry and is thus able to produce a gap in the spectral functions. The ordering wave vector, however, lies on the diagonal, while experiments report charge order at vectors $\mathbf{Q}_x$ and $\mathbf{Q}_y$ parallel to the axes of the compounds.

The goal of this paper is to examine whether a CDW with wave vectors aligned with the crystalline axes can be stabilized in the context of the EHS model. Although the EHS model is a very idealized starting point for describing the physics of cuprate superconductors, it has the merit of producing a microscopic model when SU(2) symmetry is verified at all energies. Curvature effects break the symmetry in favor of SC pairing fluctuations, while the magnetic field breaks it in favor of CDW charge order. Moreover, SU(2) symmetry is realized at only one point in the Fermi surface: at the hot spots. The understanding of how SU(2) symmetry breaks when one goes from a description of hot spots to a description of hot regions deserves a more detailed future study. Here we focus still on the EHS model, with additional short-range AFM interaction.

We introduce an original Hubbard-Stratonovich (HS) decoupling which enables us to consider the CDW order (with its pairing counterpart) and the QDW/SC order on the same footing. We find, generically, that pure QDW/SC order is stable, while the pure CDW/PDW solution is unstable. This solution is in agreement with our previous findings, as well as with several recent studies, which conclude that within the EHS model where interactions are mediated by AFM paramagnons, the only instabilities are pure d-wave diagonal orders and d-wave pairing states. In order to get any new (but weaker) instability we have to introduce an external perturbation, which we do in the present work, in the form of a short-range AFM interaction which breaks orthorhombicity. We show then that at lower temperatures a third solution emerges in which QDW/SC and CDW/PDW orders coexist [coexistence (CE) solution]. The transition towards CE is found to be weakly first order. Our conclusion is that the spin-fermion model supports the emergence of a CDW with wave vectors parallel to the axes, but in CE with a larger instability, the QDW/SC order, which is a good candidate for the PG. The magnitude of the CDW order depends on the details of the Fermi surface topology, while the QDW/SC order is insensitive to the shape of the Fermi surface. Moreover, the underlying SU(2) symmetry of the PG state enforces a degenerate PDW counterpart to the CDW order. Since the PDW lies at the hot-spot wave vector, it breaks time-reversal symmetry, which gives a natural explanation for the observation that a Kerr signal has been observed at the incipient CDW ordering transition.

II. METHOD

A. Model

Our starting point is the spin-fermion model, which can be described through the Lagrangian $L = L_\psi + L_\phi$,

where

$$L_\chi = \chi^*_{\mathbf{k}\sigma}(\partial_\tau + \epsilon_k + g\phi\sigma)\chi_{\mathbf{k}\sigma}, \tag{1a}$$

$$L_\phi = \tfrac{1}{2}\phi D^{-1}\phi + \tfrac{u}{2}(\phi^2)^2. \tag{1b}$$

L_χ is the fermion Lagrangian representing electrons with dispersion ϵ_k that are interacting with a bosonic spin excitation ϕ described in Lagrangian L_ϕ with the interacting magnitude g. The spin-wave boson ϕ propagates through

$$D^{-1}(\omega,\mathbf{q}) = \frac{\omega^2}{v_s^2} + (\mathbf{q} - \mathbf{Q})^2 + m_a, \tag{2}$$

where v_s is the spin-wave velocity, $\mathbf{Q}$ is the AFM ordering wave vector, and m_a is the spin-wave boson mass, which vanishes at the QCP.

We add to the original Lagrangian, (1a) and (1b), a small perturbation in the form of a short-range nearest-neighbor superexchange interaction,

$$L_C = \sum_{\langle i,j\rangle\sigma} \bar{J}_{i,j}\chi^\dagger_{i\sigma}\chi_{j-\sigma}\chi^\dagger_{j-\sigma}\chi_{i\sigma}, \tag{3}$$

where the notation $\langle i,j\rangle$ stands for nearest-neighbor sites. In order to simplify the study we take a bipartite modulation of $\bar{J}_{i,j}$, which, when we Fourier transform, gives

$$L_C = 2\sum_{\mathbf{k},\mathbf{k}',\sigma} \bar{J}_{\mathbf{k},\mathbf{k}'}\chi^\dagger_{\mathbf{k}\sigma}\chi_{\mathbf{k}+\mathbf{Q}-\sigma}\chi^\dagger_{\mathbf{k}'+\mathbf{Q}-\sigma}\chi_{\mathbf{k}'\sigma}$$

$$\text{with}\quad \bar{J}_{\mathbf{k},\mathbf{k}'} = \bar{J}_x\cos(k_x - k'_x) + \bar{J}_y\cos(k_y - k'_y). \tag{4}$$

Typically we choose $\bar{J}_x \neq \bar{J}_y$, which breaks the C_4 symmetry of the lattice, which we relate to a slight breaking of the orthorhombicity in real materials. $\mathbf{Q} = (\pi,\pi)$ is the AFM modulation wave vector.

We further simplify the problem by restricting and linearizing the fermion dispersion represented in Fig. 1 to the eight hot spots, which are the only points with critical scattering through the paramagnons at $T = 0$. Through such a transformation the model is essentially projected onto the EHS model. The hot spots are labeled in the 32×32 symmetry space $(\Sigma,\Lambda,L,\tau,\sigma)$, in which every subspace is described by a Pauli matrix. To simplify the notation, we do not write here the occurrence of the identity Pauli matrices in the formulas. The first three tensor products (Σ,Λ,L) describe the symmetries of the Brillouin zone, with, respectively, Σ the permutation of two hot spots inside a pair of hot spots, Λ the permutation of two pairs of hot spots inside a quartet, and L the permutation of the two quartets of hot spots, as depicted in Fig. 1. Finally, τ stands for the particle-hole, and σ for the spin space. The Fermi velocity is further linearized and written in the matrix form $\hat{\epsilon}_k = v_x\hat{x} + v_y\hat{y}$, with $\hat{x} = (k_x P_{\Sigma_x} - k_y P_{\Sigma_y})\Lambda_3 L_3$, $\hat{y} = (k_y P_{\Sigma_x} - k_x P_{\Sigma_y})\Lambda_3$, $v_x = v\cos\theta$, $v_y = v\sin\theta$, with θ the angle of the Fermi velocity with the x axis (see Fig. 1). $P_{\Sigma_x} = (1 + \Sigma_3)/2$ and $P_{\Sigma_y} = (1 - \Sigma_3)/2$ are projection operators onto the first and second components of the Σ space.

We naturally follow the notation of Ref. [52] and introduce a 32×32–fermion vector within the particle-hole τ space,

$$\psi = \frac{1}{\sqrt{2}}\begin{pmatrix}\chi^*\\i\sigma_2\chi\end{pmatrix}_\tau, \quad \psi^\dagger = \frac{1}{\sqrt{2}}(-\chi^t \quad -i\sigma_2\chi^\dagger), \tag{5}$$
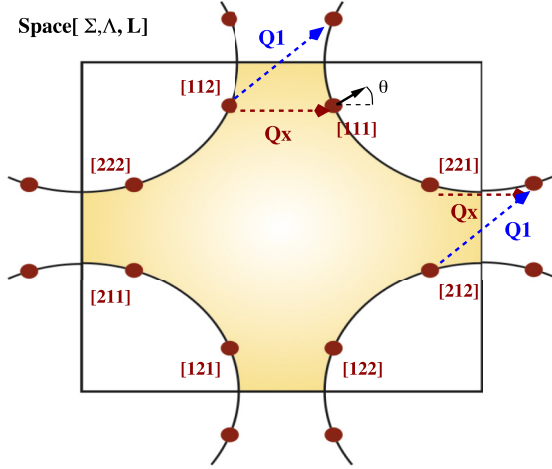
FIG. 1. (Color online) Schematic Fermi surface of cuprate superconductors in the first Brillouin zone of a square lattice. The eight hot spots are depicted by filled (red) circles labeled with the (Σ, Λ, L) space. The angle θ is defined between the velocity vector at the [111] hot spot and the x axis. The experimentally observed CDW vector $\mathbf{Q}_x$ connects the L_2 sector, whereas the diagonal QDW/SC vector Q_1 does not.

where χ^t is the simple transposition, and $\sigma_2 = \begin{pmatrix} 0 & -i \\ i & 0 \end{pmatrix}_\sigma$ is the Pauli matrix in the spin sector σ. A new conjugation is further introduced with

$$\bar{\psi} = (C\psi)^t, \quad \text{with} \quad C = \begin{pmatrix} 0 & i\sigma_2 \\ -i\sigma_2 & 0 \end{pmatrix}_\tau = -\tau_2\sigma_2, \quad (6)$$

where τ_2 is the Pauli matrix in τ space. Note that in the absence of a magnetic field and of spin-flip phenomena, the degeneracy in the spin space σ allows us to focus only on the reduced 16×16 $(\Sigma, \Lambda, L, \tau)$ space. We refer the reader to the Supplemental Material to Ref. [52] for details.

Using Eq. (1b) the spin-boson field ϕ is then formally integrated out of the partition function to get the effective partition function $Z = \int d\psi \exp(-S_0 - S_{\text{int}})$, with [here $x = (\mathbf{r}, \tau)$ and the trace Tr is taken over the 16×16 matrix space]

$$S_0 = \int dx\,dx'\, \bar{\psi}_x g_0^{-1} \psi_{x'}, \quad (7a)$$

$$S_{\text{int}} = \int dx\,dx'\, \text{Tr}(J_{x-x'}\psi_x \bar{\psi}_{x'} \Sigma_1 \psi_{x'} \bar{\psi}_x \Sigma_1), \quad (7b)$$

$$\text{with} \quad J_{x-x'} = \frac{3g^2}{2} D_{x-x'}. \quad (7c)$$

The constant $J_{x-x'}$ is chosen so that C_4 orthorhombic symmetry is broken [$J_x \neq J_y$; Eq. (7)], which then allows us to make a distinction between the two order parameters that we want to study. Note the factor Σ_1 in Eq. (7b), which comes from the translation by the AFM wave vector $\mathbf{Q} = (\pi, \pi)$ originating from the paramagnon propagator in Eq. (2). There are many ways to decouple the action of Eq. (7) into the physically relevant hydrodynamic modes of the system. The issue we face here is that the various order parameters that we want to study simultaneously have different symmetries.

B. Order parameters

The first-order parameter that we consider is our candidate for the PG phase, which we have considered in previous work [52,55,63,64]. It is a composite order parameter composed of a pairing d-wave sector and a QDW sector (QDW/SC). It is written as [52]

$$\hat{B}_1 = B_1(\epsilon_n, \mathbf{k})\hat{U}, \quad \text{with} \quad (8a)$$

$$\hat{U}_\Lambda = i\begin{pmatrix} 0 & \hat{u}_\tau \\ -\hat{u}_\tau^\dagger & 0 \end{pmatrix}_\Lambda, \quad \hat{u}_\tau = \begin{pmatrix} \Delta_- & \Delta_+ \\ -\Delta_+^* & \Delta_-^* \end{pmatrix}_\tau. \quad (8b)$$

Herein, Δ_- is the QDW component and Δ_+ is the d-wave SC component of the order parameter. They are defined as

$$\Delta_- = \langle \psi_{\mathbf{k},\sigma}^\dagger \psi_{\mathbf{k}+\mathbf{Q}_{1,2},\sigma} \rangle, \quad \Delta_+ = \langle \psi_{\mathbf{k},\sigma} \psi_{-\mathbf{k},-\sigma} \rangle, \quad (9)$$

with $\mathbf{Q}_{1,2} = (\mathbf{Q}_x \pm \mathbf{Q}_y)/2$. Note that Δ_- can be rewritten as $\Delta_- = \langle \psi_{\mathbf{k},\sigma}^\dagger \psi_{-\mathbf{k},\sigma} \rangle$, since at the hot spots, $\mathbf{Q}_{1,2} = 2\mathbf{k}_{\text{hs}}$. In this model where the Fermi surface is restricted to eight hot spots, the QDW component describing the charge order is organized along the diagonal vector, as a consequence of its pure d-wave symmetry. The SU(2) symmetry of the model is enforced, in this matrix representation, by the constraint $|\Delta_+|^2 + |\Delta_-|^2 = 1$. This constraint leads to a reduction in the two self-consistent mean-field gap equations for Δ_+ and Δ_- to only one self-consistent equation for the modulus of the order parameter B_1. A study of the temperature-doping phase diagram of the QDW/SC in the EHS model is reported in [52].

In addition to the QDW/SC order parameter, we study the possibility of a CDW order parameter with a wave vector parallel to the x, y axes defined as

$$B_2 = \langle \psi_{\mathbf{k},\sigma}^\dagger \psi_{\mathbf{k}+\mathbf{Q}_{x(y)},\sigma} \rangle. \quad (10)$$

For reasons of simplicity we consider exclusively the wave vector $\mathbf{Q}_x$, which describes a "stripe" order parameter, for the study of a less pronounced nematicity, and comparison with the checkerboard solution will be given in a forthcoming publication. A CDW organized along the $\mathbf{Q}_x$ involves some off-diagonal component in the L sector. The CDW order parameter is written in the $(\Sigma, \Lambda, L, \tau)$ space as

$$\hat{B}_2 = \begin{pmatrix} B_{2x} & 0 \\ 0 & B_{2y} \end{pmatrix}_\Sigma L_2 \otimes \Lambda_3 \otimes \hat{u}_\tau. \quad (11)$$

The notations B_{2x} and B_{2y} stand for different amplitudes allowed in the P_{Σ_x} and P_{Σ_y} sectors [corresponding, respectively, to the $(0, \pi)$ and $(\pi, 0)$ sectors]. The pure d-wave case corresponds to $B_{2x} = -B_{2y}$, while the generic case corresponds to a mixture of s- and d-wave symmetry around the Fermi surface [65]. Without any loss of generality, the CDW matrix can handle an extra $\hat{u}_\tau$ structure in the particle-hole space, with the same definition as in Eq. (8b). This amounts to rotating the CDW sector by the same SU(2) rotations as for the QDW/SC cases, producing finite-q pairing in the particle-particle channel, or PDW pairing. This type of pairing has been suggested by various groups in recent studies

of the PG state of the cuprates [68]:

$$\Delta'_- = \langle \psi^\dagger_{\mathbf{k},\sigma} \psi_{\mathbf{k}+\mathbf{Q}_x,\sigma} \rangle, \quad \Delta'_+ = \langle \psi_{\mathbf{k},\sigma} \psi_{-\mathbf{k}-\mathbf{Q}_x,-\sigma} \rangle. \quad (12)$$

When solving self-consistently for $\hat{B}_1$ and $\hat{B}_2$, the same small $\mathbf{k}$-space anisotropy must be tolerated for $\hat{B}_1$, leading to

$$\hat{B}_1 = \begin{pmatrix} B_{1x} & 0 \\ 0 & B_{1y} \end{pmatrix}_\Sigma \hat{U}_\Lambda. \quad (13)$$

C. Hubbard-Stratonovich decoupling

The problem we face when decoupling Eq. (A1) is that we would like to decouple the quadratic form naturally in a symmetric way between one factor and its conjugate, but in order to describe the two order parameters $\hat{B}_1$ and $\hat{B}_2$ on the same footing, we must find an HS transformation which allows an asymmetric decoupling in the $\bar{\psi}_x \psi_{x'}$ and $\Sigma_1 \bar{\psi}_x \Sigma_1 \psi_{x'}$ factors. In all generality, the HS decoupling can be written

$$Z = \frac{\int \mathscr{D}[\psi] \mathscr{D}[Q_a, Q_b] \, I[Q_a, Q_b, \psi] \, \exp[-S_0 - S_{\text{int}}]}{\int \mathscr{D}[Q_a, Q_b] \, I[Q_a, Q_b, 0]}, \quad (14a)$$

$$I[Q_a, Q_b, \psi] = \exp\left[-J^{-1}_{\mathbf{x}-\mathbf{x}'}(Q_a - i J_{\mathbf{x}-\mathbf{x}'} \psi_x \bar{\psi}_{x'})(Q_b - i J_{\mathbf{x}-\mathbf{x}'} \Sigma_1 \psi_{x'} \bar{\psi}_x \Sigma_1)\right]. \quad (14b)$$

In Eq. (14a) we must ensure that the quadratic form in the exponential is always positive definite and that the resulting free energy is real for any field $Q_{a,b}$. We choose $Q_a = \Sigma_1 Q^\dagger \Sigma_1$ and $Q_b = Q$. This relation defines a new charge conjugation $Q_a = \bar{Q}$, with

$$\bar{Q} = \Sigma_1 Q^\dagger \Sigma_1. \quad (15)$$

In the remainder of the paper, this conjugation is used instead of the original charge conjugation. The notion of a positive definite form inside the path integral is CDW thus defined with respect to the conjugation, Eq. (15).

D. Free energy

After the HS decomposition and integrating out of the fermions, we get the free energy

$$\frac{\Delta F}{T} = \int \text{Tr} J^{-1} (Q_a Q_b)$$

$$- \frac{1}{2} \int \text{Tr} \ln \left(g_0^{-1} + i(Q_a + \Sigma_1 Q_b \Sigma_1)\right)$$

$$= \int dx dx' \text{Tr} J^{-1}_{x-x'} (\bar{Q}_{x,x'} Q_{x',x})$$

$$- \frac{1}{2} \int dx dx' \text{Tr} \ln \left(g_0^{-1} + i(\bar{Q}_{x,x'} + \Sigma_1 Q_{x,x'} \Sigma_1)\right), \quad (16)$$

where $g_0^{-1} = i\epsilon + i\hat{\mathbf{v}} \cdot \nabla_{\mathbf{x}}$, and $Q = i\hat{B}_1 + \hat{B}_2$. Projecting Eq. (16) onto the $\Sigma_x = (1 + \Sigma_3)/2$ and $\Sigma_y = (1 - \Sigma_3)/2$ axes, we get

$$\frac{\Delta F}{T} = \frac{\Delta F_x}{T} + \frac{\Delta F_y}{T} = \int \text{Tr} \, J^{-1}_{x-x'} (\hat{\bar{B}}_x \hat{B}_x + \hat{\bar{B}}_y \hat{B}_y)$$

$$- \frac{1}{2} \int \text{Tr} \ln \left(g_{0x}^{-1} - (\hat{\bar{B}}_x + \hat{B}_y)\right)$$

$$- \frac{1}{2} \int \text{Tr} \ln \left(g_{0x}^{-1} - (\hat{\bar{B}}_y + \hat{B}_x)\right), \quad (17)$$

which can be recast into

$$\frac{\Delta F}{T} = \text{Tr} \int dx dx' J^{-1}_{x-x'} [\hat{\bar{B}}_x \hat{B}_x + \hat{\bar{B}}_y \hat{B}_y]$$

$$- \frac{1}{2} \int dx dx' \text{Tr} \ln \left(g_{0x}^{-1} - \hat{b}_x\right) + (x \leftrightarrow y), \quad (18)$$

with $\hat{b}_x = \hat{\bar{B}}_x + \hat{B}_y$, $\hat{b}_y = \hat{\bar{B}}_y + \hat{B}_x$, and $x = (\mathbf{r}, \tau)$ and $x' = (\mathbf{r}', \tau')$ denoting the set of coordinates, whereas $\hat{B}_x$ and $\hat{g}_x$ denote the projection onto the Σ_x and Σ_y axes.

In order to convince ourselves that the new conjugation is giving physically meaningful results, we write the MFE by differentiating sequentially with respect to $\bar{B}_{x,x'}$ and $B_{x,x'}$. We get

$$J^{-1}_{x-x'} \hat{B}_x = -\frac{1}{2} \text{Tr} [\hat{g}_x], \quad (19a)$$

$$J^{-1}_{x-x'} \hat{\bar{B}}_x = -\frac{1}{2} \text{Tr} [\hat{g}_y], \quad (19b)$$

$$J^{-1}_{x-x'} \hat{B}_y = -\frac{1}{2} \text{Tr} [\hat{g}_y], \quad (19c)$$

$$J^{-1}_{x-x'} \hat{\bar{B}}_y = -\frac{1}{2} \text{Tr} [\hat{g}_x], \quad (19d)$$

with $\hat{g}_x = (g_{0x}^{-1} + \hat{b}_x)^{-1}$ and $\hat{g}_y = (g_{0y}^{-1} + \hat{b}_y)^{-1}$. We see that in order for the MFE to have a solution, we need to impose

$$\hat{\bar{B}}_x = \hat{B}_y, \quad (20a)$$

$$\hat{\bar{B}}_y = \hat{B}_x, \quad (20b)$$

which works as a condition of reality for the HS fields. Later on we look for solutions of the MFE for fields real with respect to the old conjugation $\bar{B} = \Sigma_1 B \Sigma_1$, $(B^\dagger = B)$.

It turns out that the matrices structure inside the free energy can be reduced using the trick that for all $M = \begin{pmatrix} A & D \\ C & B \end{pmatrix}$

$$\det(M) = \det B \det(A - D B^{-1} C), \quad (21)$$

where A,B,C,D are matrices. The intermediate steps are summarized in Appendix A. The final result for the free energy is

$$F_0 = T \sum_\epsilon \int dx dx' J^{-1}_{x-x'} [\bar{B}_{1x} B_{1x} + \bar{B}_{1y} B_{1y}$$

$$+ \bar{B}_{2x} B_{2x} + \bar{B}_{2y} B_{2y}], \quad (22a)$$

$$F_x = -\frac{1}{2} T \sum_\epsilon \int dx dx' [-\ln(d_x - b_{2x}^2) + \ln((\epsilon^2 + b_{1x}^2) d_x^2$$

$$+ (v p_x \cos\theta d_x + v p_y \sin\theta (d_x - 2b_{2x}^2))^2)], \quad (22b)$$

$$F_y = -\frac{1}{2}T\sum_\epsilon \int dx\, dx' \big[-\ln\big(d_y - b_{2y}^2\big) + \ln\big((\epsilon^2 + b_{1y}^2)d_y^2$$
$$+ \big(vp_x \sin\theta\, d_y + vp_y \cos\theta\big(d_y - 2b_{2y}^2\big)\big)^2\big)\big],$$

$$d_x = \epsilon^2 + (vp_x \cos\theta - vp_y \sin\theta)^2 + b_{1x}^2 + b_{2x}^2,$$

$$d_y = \epsilon^2 + (vp_x \sin\theta - vp_y \cos\theta)^2 + b_{1y}^2 + b_{2y}^2,$$

$$b_{ix} = \overline{B}_{ix} + B_{iy}, \quad b_{iy} = \overline{B}_{iy} + B_{ix}, \quad i = 1,2. \tag{22c}$$

Equations (22) and the introduction of the new conjugation Eq. (15) constitute the main technical tools of this paper which enable a controlled discussion of the CE and interplay of the two order parameters $\hat{B}_1$ (QDW/SC) and $\hat{B}_2$ (CDW).

To derive self consistency equations for the four order parameters $\overline{B}_x, \overline{B}_y$ and B_x, B_y we differentiate the free energy with respect to $\overline{B}_x, \overline{B}_y$ and B_x, B_y successively (cf. Appendix B). In order to perform this task one must Fourier transform equations of the type Eq. (19a):

$$J_{x-x'}^{-1} B_{x,x'} = -\frac{1}{2}\mathrm{Tr}\big[g_0^{-1} + b_{x,x'}\big]. \tag{23}$$

From Eq. (7c) we see that $J_{x-x'}^{-1}$ depends on the paramagnon propagator $D_{x-x'}$. We multiply both sides by $J_{x-x'}$, and after Fourier transforming and integrating over the $\mathbf{q}$, we get

(cf. Appendix B)

$$B_{\mathbf{k},\mathbf{k}+\mathbf{P}} = -\frac{1}{2}\mathrm{Tr}\sum_\mathbf{q} J_\mathbf{q}\big[g_0^{-1} + b_{\mathbf{k},\mathbf{k}+\mathbf{P}+\mathbf{q}}\big]. \tag{24}$$

The orders introduced in Eqs. (9) and (10) correspond to $\mathbf{P} = \mathbf{Q}_{1,2}$ and $\mathbf{P} = \mathbf{Q}_{x,y}$ respectively while the short hand notation $B_\mathbf{k} = B_{\mathbf{k},\mathbf{k}+\mathbf{P}}$ and $b_\mathbf{k} = b_{\mathbf{k},\mathbf{k}+\mathbf{P}}$ have been used.

The final result for the mean-field equations (MFEs) is

$$B_{1x}(\epsilon_n) = 4\gamma_1 T \sum_{\epsilon'} A_{1x}(\epsilon_n, \epsilon_n') B_{1y}(\epsilon_n'), \tag{25a}$$

$$B_{1y}(\epsilon_n) = 4\gamma_1 T \sum_{\epsilon'} A_{1y}(\epsilon_n, \epsilon_n') B_{1x}(\epsilon_n'), \tag{25b}$$

$$B_{2x}(\epsilon_n) = 4\gamma_2 T \sum_{\epsilon'} A_{2x}(\epsilon_n, \epsilon_n') B_{2y}(\epsilon_n'), \tag{25c}$$

$$B_{2y}(\epsilon_n) = 4\gamma_2 T \sum_{\epsilon'} A_{2y}(\epsilon_n, \epsilon_n') B_{2x}(\epsilon_n'), \tag{25d}$$

where $\gamma_1 = 3g_1^2/2$ and $\gamma_2 = 3g_2^2/2$ are coupling constants which can be slightly different from each other due to the breaking of anisotropy [cf. Eq. (14a)], and the parameters A_{1x}, A_{1y}, A_{2x}, and A_{2y} are given by

$$A_{1x} = \sum_\mathbf{q} \frac{D_{\omega,\mathbf{q}}}{V} \left(\frac{d_x + 2vq_x vq_y \cos\theta \sin\theta}{d_x^2 + 4vq_x vq_y \cos\theta \sin\theta\, d_x - 4b_{2x}^2 v^2 q_y^2 \sin^2\theta} \right), \tag{26a}$$

$$A_{2x} = \sum_\mathbf{q} \frac{D_{\omega,\mathbf{q}}}{V} \left(\frac{d_x + 2vq_x vq_y \cos\theta \sin\theta - 2v^2 q_y^2 \sin^2\theta}{d_x^2 + 4vq_x vq_y \cos\theta \sin\theta\, d_x - 4b_{2x}^2 v^2 q_y^2 \sin^2\theta} \right), \tag{26b}$$

$$A_{1y} = \sum_\mathbf{q} \frac{D_{\omega,\mathbf{q}}}{V} \left(\frac{d_y + 2vq_x vq_y \cos\theta \sin\theta}{d_y^2 + 4vq_x vq_y \cos\theta \sin\theta\, d_y - 4b_{2y}^2 v^2 q_y^2 \cos^2\theta} \right), \tag{26c}$$

$$A_{2y} = \sum_\mathbf{q} \frac{D_{\omega,\mathbf{q}}}{V} \left(\frac{d_y + 2vq_x vq_y \cos\theta \sin\theta - 2v^2 q_y^2 \cos^2\theta}{d_y^2 + 4vq_x vq_y \cos\theta \sin\theta\, d_y - 4b_{2y}^2 v^2 q_y^2 \cos^2\theta} \right), \tag{26d}$$

$$\text{with} \quad D_{\omega,\mathbf{q}} = \big(\gamma |\omega| + q_x^2 + q_y^2 + m_a\big),$$

where $\frac{1}{V}\sum_\mathbf{q} \equiv \int \frac{d\mathbf{q}}{(2\pi)^2}$. Note that the form of the propagator $D_{\omega,\mathbf{q}}$ has slightly changed compared to Eq. (2) since we consider Landau damping. A closer look at Eq. (26) shows that the right-hand side of (25a) and (25d) is always lower than the right-hand side of (25b) and (25c), respectively. In order for the two solutions to exist simultaneously, it is enough to introduce a slightly different coefficient J_2 in front of (25b) and (25d), with $g_2 \geqslant g_1$, which henceforth will favor the B_2 type of decoupling. This difference can be introduced through a small perturbation like the breaking of the C_4 symmetry.

The typical result of the MFEs for parameters $g_2 \simeq g_1$ is shown in Fig. 2. We observe that three solutions are obtained: (i) the pure QDW/SC solution, for which $B_1 \neq 0$ and $B_2 = 0$; (ii) the pure CDW/PDW solution, for which $B_2 \neq 0$ and $B_1 = 0$; and (iii) the CE solution, where $B_1 \neq 0$ and $B_2 \neq 0$. Moreover, for typical values of the coupling constants, solutions i and ii have similar magnitudes, while for the CE

solution $B_2 \ll B_1$. The dependence on the Fermi velocity angle θ, which captures the dependence of the solutions on the fermiology of the compounds, is depicted in Fig. 3. We find that the pure QDW/SC solution (i) is insensitive to fermiology, whereas the pure CDW/PDW solution (ii) is more favorable when $\theta = 0$, which corresponds to flat portions of the Fermi surface in the antinodal region. The insensitivity of the QDW/SC solution to the value of θ stems from the fact that, in our matrix framework $\{\hat{B}_1, \hat{\epsilon}_k\} = 0$, which is not the case for the CDW/PDW order. It is summarized here by saying that the QDW/SC phase is much less sensitive to the fermiology than the CDW/PDW phase [39].

E. Stability analysis

To analyze the stability of the solutions, we include Gaussian fluctuations. We expand Eq. (22) to second order
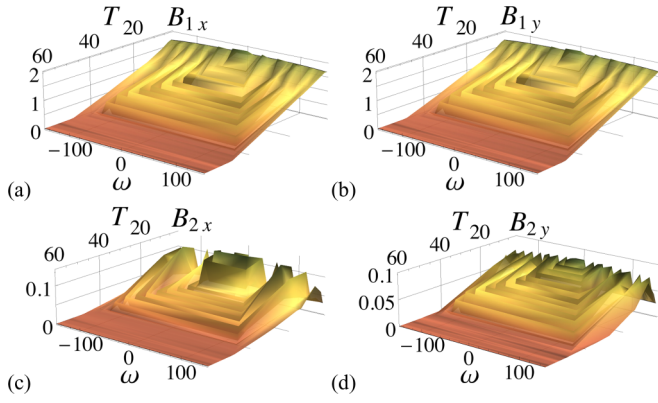
FIG. 2. (Color online) Typical form of the order parameters in the CE phase as a function of the frequency ω and temperature T: $B_{1x/1y}$ (a, b), representing QDW/SC; and $B_{2x/2y}$ (c, d), representing CDW/PDW order. Note that the CDW/PDW component is one order of magnitude smaller than the QDW/SC solution. We take g_1 slightly bigger than g in order to stabilize the CDW sector. The actual figure corresponds to $g_1 = 20$, $g_2 = 30$, $v = 6$, $m_a = 0.1$, $\gamma = 3$, and $W = 2\pi$, where W is the bandwidth of integration in **k** space and $\theta = 0.1$.

in the fluctuation field δB_{1x}, δB_{1y}, δB_{2x}, δB_{2y}, and their conjugate. We find (see Appendix C for details)

$$\Delta F = \frac{T}{V} \sum_{\epsilon} \sum_{\mathbf{k},\mathbf{k}'} \sum_{i=1}^{2} \left[J_{\mathbf{k}-\mathbf{k}'}^{-1} \delta \overline{B}_{ix,\mathbf{k}} \delta B_{ix,\mathbf{k}'} \right.$$
$$\left. - \left(\frac{A_{ix,\mathbf{k}} - \delta A_{ix,\mathbf{k}}}{4} \right) \delta b_{ix,\mathbf{k}}^2 \delta_{\mathbf{k},\mathbf{k}'} \right], \qquad (27)$$

with $\delta b_{ix} = \delta \overline{B}_{ix} + \delta B_{iy}$. In order to study the stability of the various solution, we write the quadratic form,

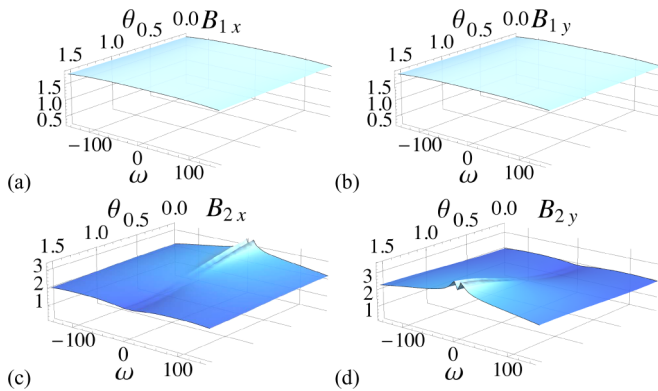$$\Delta F = \frac{1}{2} \sum_{i=1}^{2} \Psi_i^{\dagger} M_i \Psi_i, \qquad (28)$$

FIG. 3. (Color online) Typical form of the order parameters in the CE phase as a function of the frequency ω and velocity angle θ: $B_{1x/1y}$ (a, b), representing QDW/SCl and $B_{2x/2y}$ (c, d), representing CDW/PDW order. Note that the CDW/PDW component is one order of magnitude smaller than the QDW/SC solution. Parameters are the same as in Fig. 2.

with $\Psi_i = (\delta B_{ix}, \delta \overline{B}_{iy}, \delta \overline{B}_{ix}, \delta B_{iy})^T$ and $\Psi_i^{\dagger} = (\delta B_{ix}, \delta \overline{B}_{iy}, \delta \overline{B}_{ix}, \delta B_{iy})$. The stability matrix M is written

$$M_i = \begin{pmatrix} J_{\mathbf{k}-\mathbf{k}'}^{-1} & 0 & \overline{A}_{ix} & \overline{A}_{ix} \\ 0 & J_{\mathbf{k}-\mathbf{k}'}^{-1} & \overline{A}_{ix} & \overline{A}_{ix} \\ \overline{A}_{iy} & \overline{A}_{iy} & J_{\mathbf{k}-\mathbf{k}'}^{-1} & 0 \\ \overline{A}_{iy} & \overline{A}_{iy} & 0 & J_{\mathbf{k}-\mathbf{k}'}^{-1} \end{pmatrix}, \qquad (29)$$

with $\overline{A}_{ix} = (A_{ix} - \delta A_{ix})/2$ and $\overline{A}_{iy} = (A_{iy} - \delta A_{iy})/2$. The stability condition corresponds to the condition for which M is positive definite. This condition is equivalent to det $M \geqslant 0$, which leads to

$$J_{\mathbf{k}-\mathbf{k}'}^{-2} - 4\overline{A}_{ix}\overline{A}_{iy} \geqslant 0. \qquad (30)$$

Note that the free energy (27) is always real. When $\delta A_{ix} = 0$, Eq. (30) is equivalent to the condition for the existence of MF solutions [Eqs. (25)]. The stability conditions in the respective directions $B_{1x(y)}$ and $B_{2x(y)}$ are presented in Fig. 4. Typically, one observes that the pure QDW/SC solution is stable [Figs. 4(a$_1$) and 4(a$_2$)], while the pure CDW/PDW solution is unstable [Figs. 4(b$_1$) and 4(b$_2$)]. The CE solution is always stable at low temperatures [Figs. 4(c$_1$) and 4(c$_2$)].

In order to differentiate between the two stable solutions (pure QDW/SC and CE) we evaluate the free energy in Fig. 5. We see that the CE solution is slightly lower than the pure QDW/SC solution. This behavior is also observed in the limit $J_2 \gg J_1$. Our conclusion is that the generic tendency is a transition of slightly first order towards the CE solution at lower temperatures.
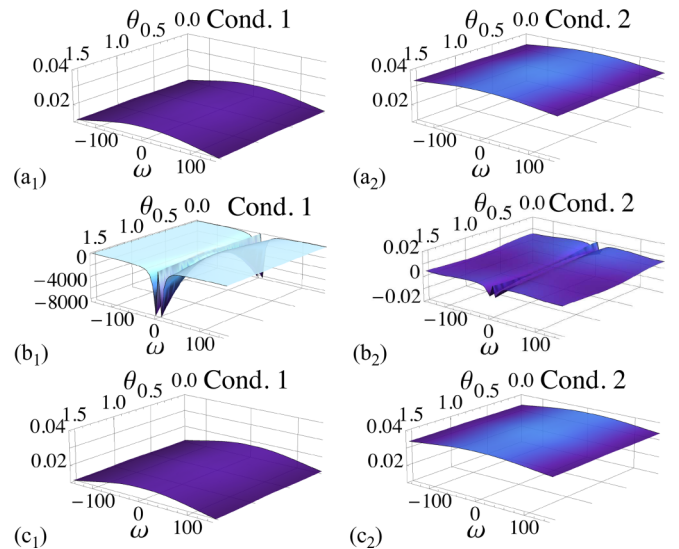

FIG. 4. (Color online) Stability conditions [left-hand side of Eq. (30)] as a function of the frequency ω and velocity angle θ for the three possible solutions in the B_1 and B_2 directions: pure QDW/SC solution [a$_1$ (dir. B_1) and a$_2$ (dir. B_2)]; pure CDW/PDW solution [b$_1$ (dir. B_1) and b$_2$ (dir. B_2)]; and CE solution (c$_1$ and c$_2$). Note that the pure CDW/PDW solution is always unstable, while the CE solution is stable. Parameters are the same as in Fig. 3.
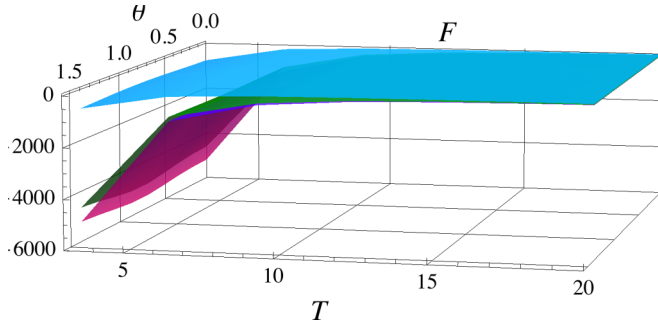
FIG. 5. (Color online) Free energy F of the three MF solutions as a function of θ and T: pure CDW/PDW (blue area), pure QDW/SC (green area), and CE (magenta area). Note that the free energy for the CE solution is slightly lower than that for both the QDW/SC and the CDW/PDW solutions. Parameters are the same as in Fig. 2.

FIG. 6. (Color online) Schematic phase diagram for high-temperature cuprate superconductors as a function of the temperature T and hole doping x. The different types of order are antiferromagnetic (AFM), quadrupole density wave (QDW), pairing density wave (PDW), charge density wave (CDW), and superconductivity (SC).

III. DISCUSSION

In the present work we have addressed the role and presence of charge order in the PG phase, in the context of an emerging SU(2) symmetry relating the charge and paring sectors. The EHS model, where the Fermi velocity has been linearized, provides a microscopic theory by which the SU(2) symmetry is verified at all energies [50–52]. Namely, in this model the Peierls and the pairing channels are degenerate. Many effects break the SU(2) symmetry in more realistic models for high-temperature superconductors. Curvature, on the one hand, favors the emergence of the superconducting state at low temperatures, while, on the other hand, application of an external magnetic field and, also, the growth of Umklapp terms in the wake of the Mott-insulating transition act in favor of the charge sector. The generic phase diagram envisioned for cuprate SC is one in which the SU(2) symmetry is "lightly broken" in the sense that the splitting of the charge and pairing sectors is much smaller than their mean value. While at low temperatures the lower energy state is, for example, of SC order, thermal effects then excite the system to fill the higher energy state [52]. We identify the temperature at which SU(2) symmetry exists between short-range SC pairing fluctuations and QDW order as the PG temperature T^*, depicted in Fig. 6. As a composite order parameter made of two distinct short-range components, this order has the potential to gap out the antinodal part of the Fermi surface while leaving "cold" the nodal part. Such a treatment requires starting with a more realistic model going beyond the EHS treatment of the Fermi surface. The PG phase occurs as a preemptive instability around the AFM QCP of itinerant electrons. The feedback of such an instability on the long-range AFM modes is to self-consistently gap them out, effectively producing a short-range AFM correlation (hence pushing back the QCP) to the left of the phase diagram. As a result, the PG state in this model is constituted of short-range AFM correlations coexisting with SU(2)-symmetric short-range d-wave SC preformed pairs and a CDW. A recent two-loop RG study precisely confirmed that such a fixed point exists in the EHS model [66].

For a very long time three main players were identified in the physics of cuprate superconductors: antiferromagnetism, d-wave SC, and the Mott metal-insulator transition. Within the SU(2) scenario a fourth player enters the game: charge
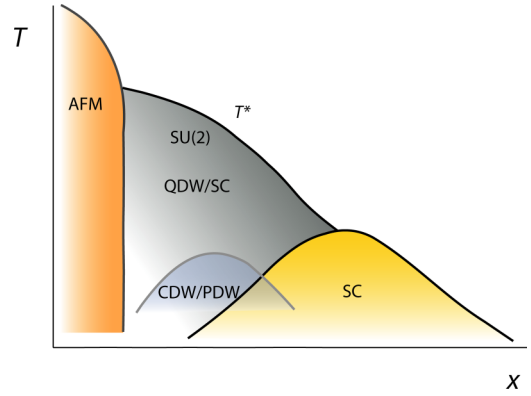
order. The assertion that d-wave charge order and pairing SC are quasidegenerate in the cuprate family has long-range consequences and enables us to classify the compounds via their SU(2) character. For example, in La-based compounds, due to the presence of the very strong Umklapp interactions, the SU(2) symmetry is broken in favor of the charge sector, whereas YBCO, Bi2212, and Hg-1201 see the balance towards SC restored and are thus closer to the SU(2) symmetric case. Interestingly, as the doping is decreased starting from the optimally doped case in the SC state, the proliferation of Umklapp terms drive the systems towards charge ordering, very likely producing a level crossing between QDW and SC states. One can thus conjecture that an SU(2)-symmetric point is naturally present in the underdoped compounds.

We turn now to the discussion of the $\mathbf{Q}_x/\mathbf{Q}_y$ CDW recently observed experimentally. It is now a consensus in the community that the $\mathbf{Q}_{x/y}$ CDW is distinct from the PG phase and is "not" the gapping-out factor of the Fermi surface but, rather, a subsidiary instability occurring on top of an already formed PG state [24,39]. This conclusion is in agreement with the findings of the present study, where the incipient CDW is obtained in CE, but at a lower temperature than the PG state (see Fig. 6). It is found that while the PG state is insensitive to the fermiology, the temperature at which CDW order occurs and its magnitude depend strongly on its surroundings (disorder, orthorhombicity, or a peculiar form of the Fermi surface).

An important question raised within various models, including the EHS model, is how to get a CDW ordering wave vector parallel to the x and y axes, and not on the diagonal. Simple Hartree-Fock evaluations generically produce charge-ordering wave vectors on the diagonal at $(\mathbf{Q}_x \pm \mathbf{Q}_y)/2$ [53,67], and similarly for the solution of the gap equation for the QDW/SC solution [52,63], whereas nothing is observed in this direction. To resolve this discrepancy, some works have introduced Coulomb interactions [44,45], but the wave vector is still a bit tilted. Another interesting proposal is to use the three-band model and evaluate the charge response on top of an AFM PG [46], which was recently reformulated for a

spin-liquid-type PG [58]. We have also suggested using SC fluctuation to stabilize the CDW with the correct wave vector at the antinodes [64]. Recently, a work closely related to ours has suggested that a CDW occurs directly at the hot spots [54]. Our findings agree with Ref. [54] in the understanding that a competition exists at the hot spots between the CDW and the QDW/SC. However, we find that even when the coupling constants are tuned so that the CDW ordering is extremely favorable, at lower temperatures the QDW/SC re-emerges to form a CE solution. In our work, a small breaking of tetragonal symmetry (orthorhombicity) is responsible in the stabilization of a CDW/PDW as a subleading instability. It can nicely be related to the observation that in compounds where a tetragonal environment is present, as in Hg-1201, the CDW signal is very weak, almost undetectable, while in more orthorhombic compounds like YBCO, the CDW signal is stronger.

Finally, a very interesting point of the emerging SU(2) symmetry presented in this paper is that the CDW order occurs under the SU(2) dome below T^*. As such, it possesses an SU(2)-degenerate counterpart in the form of a pairing density wave (PDW) at finite wave vector. Hence the denomination CDW/PDW order. This type of order has been intensely studied recently as a potential candidate for the PG phase, based on the interpretation of ARPES data in Bi-2201 [68–70]. Within the SU(2) scenario, the PDW state is present: not as the main instability producing the PG state, but as the smallest instability in a "logarithmic hierarchy." From the itinerant electron point of of view its logarithmic divergence is always cut off by the finite-pairing wave vector, hence even in the linearized EHS model the PDW instability is subsidiary, and not the leading one. It is interesting to note that, in accordance with the observation in Refs. [54] and [69], if the $\mathbf{Q} \leftrightarrow -\mathbf{Q}$ symmetry is broken, within the CDW/PDW state, then time-reversal symmetry is broken, leading to the possibility of observing a Kerr signal below T_{CDW} [30] and possibly explaining the presence of loop currents below T^* [33,34].

In conclusion, within a detailed investigation of the eight-hot-spot model we show that charge ordering with the correct wave vector can only occur on top of a pre-existing order which is our candidate for the PG. Our conclusion is that CDW/PDW order can be stabilized at the hot spots in the spin-fermion model in CE with the QDW/SC solution. The CDW/PDW can be considered as a by-product of the emergence of QDW/SC order. Its magnitude peaks at T_c and nonlinear σ models uniting QDW and SC [52,56,63] to explain sound experiments and x-rays findings are still valid.

APPENDIX A: REDUCTION OF THE FREE ENERGY

We give here the essential steps in the reduction of the free energy. For further details about the notation, we refer the reader to the Supplemental Material to our previous paper [52]. Using Eq. (15) and setting $Q_x = i\hat{B}_x$, $Q_y = i\hat{B}_y$ ($\bar{Q}_x = -i\hat{B}_x, \bar{Q}_y = -i\hat{B}_y$), the free energy becomes

$$F = F_0 + F_x + F_y, \tag{A1a}$$

$$F_0 = T \sum_\epsilon \int \frac{d\mathbf{p}}{(2\pi)^2} J_{\mathbf{x}-\mathbf{x}'}^{-1} [\bar{\hat{B}}_x \hat{B}_x + \bar{\hat{B}}_y \hat{B}_y], \tag{A1b}$$

$$F_x = -\frac{1}{2} T \sum_\epsilon \int \frac{d\mathbf{p}}{(2\pi)^2} \text{Tr} \ln \left(g_{0x}^{-1} - \hat{b}_{1x} - \hat{b}_{2x} \right), \tag{A1c}$$

$$F_y = -\frac{1}{2} T \sum_\epsilon \int \frac{d\mathbf{p}}{(2\pi)^2} \text{Tr} \ln \left(g_{0xy}^{-1} - \hat{b}_{1y} - \hat{b}_{2y} \right), \tag{A1d}$$

with $g_{0x}^{-1} = i\epsilon - \hat{x}_\mathbf{p}$, $\hat{x}_\mathbf{p} = v p_x \cos\theta \Lambda_3 L_3 + v p_y \sin\theta \Lambda_3$, $g_{0y}^{-1} = i\epsilon - \hat{y}_\mathbf{p}$, $\hat{y}_\mathbf{p} = -v p_x \sin\theta \Lambda_3 L_3 - v p_y \cos\theta \Lambda_3$, $\hat{b}_x = \bar{\hat{B}}_x + \hat{B}_y$, and $\hat{b}_y = \bar{\hat{B}}_y + \hat{B}_x$. Using $\text{Tr} \ln G^{-1} = \ln \det G^{-1}$, where $G^{-1} = g_{0x}^{-1} - \hat{b}_{1x} - \hat{b}_{2x}$ ($G^{-1} = g_{0y}^{-1} - \hat{b}_{1y} - \hat{b}_{2y}$), and the formula

$$\det(M) = \det B \det(A - DB^{-1}C) \quad \text{for all} \quad M = \begin{pmatrix} A & D \\ C & B \end{pmatrix}, \tag{A2}$$

where A, B, C, and D are matrices, we are able to express the free energy in scalar form. In the direction Σ_x we find

$$
\begin{aligned}
M_x &= i\epsilon + (\hat{\mathbf{v}}\mathbf{p})_{\Sigma_x} - b_{1x}\Lambda_2 - b_{2x}L_2\Lambda_3 \\
&= \begin{pmatrix} M_1^a & ib_{2x}\Lambda_3 \\ -ib_{2x}\Lambda_3 & M_1^b \end{pmatrix}_L,
\end{aligned}
\tag{A3}
$$

with

$$M_1^a = i\epsilon + v p_x \cos\theta \Lambda_3 + v p_y \sin\theta \Lambda_3 - b_{1x}\Lambda_2, \tag{A4a}$$

$$M_1^b = i\epsilon - v p_x \cos\theta \Lambda_3 + v p_y \sin\theta \Lambda_3 - b_{1x}\Lambda_2, \tag{A4b}$$

which leads to

$$\det M = \det M_1^b \det M_1, \tag{A5a}$$

$$M_1 = M_1^a - b_{2x}^2 \Lambda_3 \left(M_1^b\right)^{-1} \Lambda_3. \tag{A5b}$$

We now decompose once again with

$$
\begin{aligned}
M_1 &= (i\epsilon - b_{1x}\Lambda_2 + v p_x \cos\theta \Lambda_3)(1 + \bar{d}_2) \\
&\quad + v p_y \sin\theta \Lambda_3 (1 - \bar{d}_2),
\end{aligned}
\tag{A6a}
$$

$$\bar{d}_2 = \frac{b_{2x}^2}{\epsilon^2 + \left(v p_x \cos\theta - v p_y \sin\theta\right)^2 + b_{1x}^2}, \tag{A6b}$$

$$M_1 = \begin{pmatrix} M_2^a & ib_{1x}(1 + \bar{d}_2) \\ -ib_{1x}(1 + \bar{d}_2) & M_2^b \end{pmatrix}_\Lambda, \quad \text{with} \tag{A6c}$$

$$M_2^a = (i\epsilon + v p_x \cos\theta)(1 + \bar{d}_2) + v p_y \sin\theta (1 - \bar{d}_2), \tag{A6d}$$

$$M_2^b = (i\epsilon - v p_x \cos\theta)(1 + \bar{d}_2) - v p_y \sin\theta (1 - \bar{d}_2). \tag{A6e}$$

We get

$$\det M_x = \det M_1^b \det M_2^b \det M_2, \tag{A7a}$$

$$M_2 = M_2^a - \frac{b_{1x}^2 (1 + \bar{d}_2)^2}{(i\epsilon - vp_x \cos\theta)(1 + \bar{d}_2) - vp_y \sin\theta (1 + \bar{d}_2)}. \tag{A7b}$$

We finally obtain

$$\det M_x = \frac{(\epsilon^2 + b_{1x}^2)d_x^2 + (vp_x \cos\theta\, d_x + vp_y \sin\theta (d_x - 2b_{2x}^2))^2}{d_x - b_{2x}^2}, \tag{A8a}$$

$$d_x = \epsilon^2 + (vp_x \cos\theta - vp_y \sin\theta)^2 + b_{1x}^2 + b_{2x}^2. \tag{A8b}$$

Reducing in the same manner the projection onto the Σ_y axis, and noting that we get the right formulas by shifting $\theta \to \pi/2 - \theta$, we have

$$\det M_y = \frac{(\epsilon^2 + b_{1y}^2)d_y^2 + (vp_x \sin\theta\, d_y + vp_y \cos\theta (d_y - 2b_{2y}^2))^2}{d_y - b_{2y}^2}, \tag{A9a}$$

$$d_y = \epsilon^2 + (vp_x \sin\theta - vp_y \cos\theta)^2 + b_{1y}^2 + b_{2y}^2, \tag{A9b}$$

and we finally get Eq. (22) for the free energy.

APPENDIX B: DERIVATION OF THE MEAN-FIELD EQUATIONS

The MFEs are derived by differentiation of the free energy, Eq. (A1), with respect to $\bar{B}_{x,y}$ and $B_{x,y}$ successively. We get

$$J_{\mathbf{x}-\mathbf{x'}}^{-1} \hat{B}_x = -\frac{1}{2}\mathrm{Tr}[\hat{g}_x], \tag{B1a}$$

$$J_{\mathbf{x}-\mathbf{x'}}^{-1} \bar{\hat{B}}_x = -\frac{1}{2}\mathrm{Tr}[\hat{g}_y], \tag{B1b}$$

$$J_{\mathbf{x}-\mathbf{x'}}^{-1} \hat{B}_y = -\frac{1}{2}\mathrm{Tr}[\hat{g}_y], \tag{B1c}$$

$$J_{\mathbf{x}-\mathbf{x'}}^{-1} \bar{\hat{B}}_y = -\frac{1}{2}\mathrm{Tr}[\hat{g}_x], \tag{B1d}$$

$$\hat{g}_x = (g_{0x}^{-1} + \hat{b}_x)^{-1}, \quad \hat{g}_y = (g_{0y}^{-1} + \hat{b}_y)^{-1}. \tag{B1e}$$

We see that when the MFEs do have a solution, Eq. (B1a) reduces identically to Eq. (B1d), and Eq. (B1b) reduces to Eq. (B1c). Two constraints are naturally obtained:

$$\bar{\hat{B}}_x = \hat{B}_y, \quad \bar{\hat{B}}_y = \hat{B}_x. \tag{B2}$$

The constraints, (B2), correspond to a condition of reality for the fields $\hat{B}_x$ ($\hat{B}_y$) within the conjugation operation introduced in (15). Multiplying both sides of Eqs. (B1a)–(B1d) by $J_{x-x'}$ we get

$$\hat{B}_x = -\frac{1}{2} J_{x-x'} \mathrm{Tr}[\hat{g}_x], \tag{B3}$$

$$\bar{\hat{B}}_x = -\frac{1}{2} J_{x-x'} \mathrm{Tr}[\hat{g}_y], \tag{B4}$$

$$\hat{B}_y = -\frac{1}{2} J_{x-x'} \mathrm{Tr}[\hat{g}_y], \tag{B5}$$

$$\bar{\hat{B}}_y = -\frac{1}{2} J_{x-x'} \mathrm{Tr}[\hat{g}_x], \tag{B6}$$

which, after Fourier transforming, leads to

$$T \sum_{\epsilon_n,\mathbf{k}} \hat{B}_{x,\mathbf{k},\mathbf{k+P}} = -\frac{T^2}{2}\mathrm{Tr} \sum_{\epsilon_n,\mathbf{k},\omega_n,\mathbf{q}} J_{\omega_n,\mathbf{q}}[\hat{g}_{x,\mathbf{k},\mathbf{k+P+q}}], \tag{B7}$$

$$T \sum_{\epsilon_n,\mathbf{k}} \bar{\hat{B}}_{x,\mathbf{k},\mathbf{k+P}} = -\frac{T^2}{2}\mathrm{Tr} \sum_{\epsilon_n,\mathbf{k},\omega_n,\mathbf{q}} J_{\omega_n,\mathbf{q}}[\hat{g}_{y,\mathbf{k},\mathbf{k+P+q}}], \tag{B8}$$

$$T \sum_{\epsilon_n,\mathbf{k}} \hat{B}_{y,\mathbf{k},\mathbf{k+P}} = -\frac{T^2}{2}\mathrm{Tr} \sum_{\epsilon_n,\mathbf{k},\omega_n,\mathbf{q}} J_{\omega_n,\mathbf{q}}[\hat{g}_{y,\mathbf{k},\mathbf{k+P+q}}], \tag{B9}$$

$$T \sum_{\epsilon_n,\mathbf{k}} \bar{\hat{B}}_{y,\mathbf{k},\mathbf{k+P}} = -\frac{T^2}{2}\mathrm{Tr} \sum_{\epsilon_n,\mathbf{k},\omega_n,\mathbf{q}} J_{\omega_n,\mathbf{q}}[\hat{g}_{x,\mathbf{k},\mathbf{k+P+q}}]. \tag{B10}$$

In a similar way, differentiating Eq. (22) with respect to b_{1x}, b_{1y}, b_{2x}, and b_{2y} gives four independent gap equations:

$$\gamma_1^{-1} B_{1x} = -T \sum_\epsilon \int \frac{d\mathbf{p}}{(2\pi)^2} \hat{D} \frac{\partial F_x}{\partial b_{1x}}, \tag{B11a}$$

$$\gamma_1^{-1} B_{1y} = -T \sum_\epsilon \int \frac{d\mathbf{p}}{(2\pi)^2} \hat{D} \frac{\partial F_y}{\partial b_{1y}}, \tag{B11b}$$

$$\gamma_2^{-1} B_{2x} = -T \sum_\epsilon \int \frac{d\mathbf{p}}{(2\pi)^2} \hat{D} \frac{\partial F_x}{\partial b_{2x}}, \tag{B11c}$$

$$\gamma_2^{-1} B_{2y} = -T \sum_\epsilon \int \frac{d\mathbf{p}}{(2\pi)^2} \hat{D} \frac{\partial F_y}{\partial b_{2y}}, \tag{B11d}$$

$$\gamma_1 = \frac{3g_1^2}{2}, \quad \gamma_2 = \frac{3g_2^2}{2}. \tag{B11e}$$

It is useful to introduce the notations ($x_1 = b_{1x}^2$, $x_2 = b_{2x}^2$, $y_1 = b_{1y}^2$, $y_2 = b_{2y}^2$)

$$A_{1x} = -\int \frac{d\mathbf{p}}{(2\pi)^2} \hat{D} \frac{\partial F_x}{\partial x_1}, \tag{B12a}$$

$$A_{2x} = -\int \frac{d\mathbf{p}}{(2\pi)^2} \hat{D} \frac{\partial F_x}{\partial x_2}, \tag{B12b}$$

$$A_{1y} = -\int \frac{d\mathbf{p}}{(2\pi)^2} \hat{D} \frac{\partial F_y}{\partial y_1}, \tag{B12c}$$

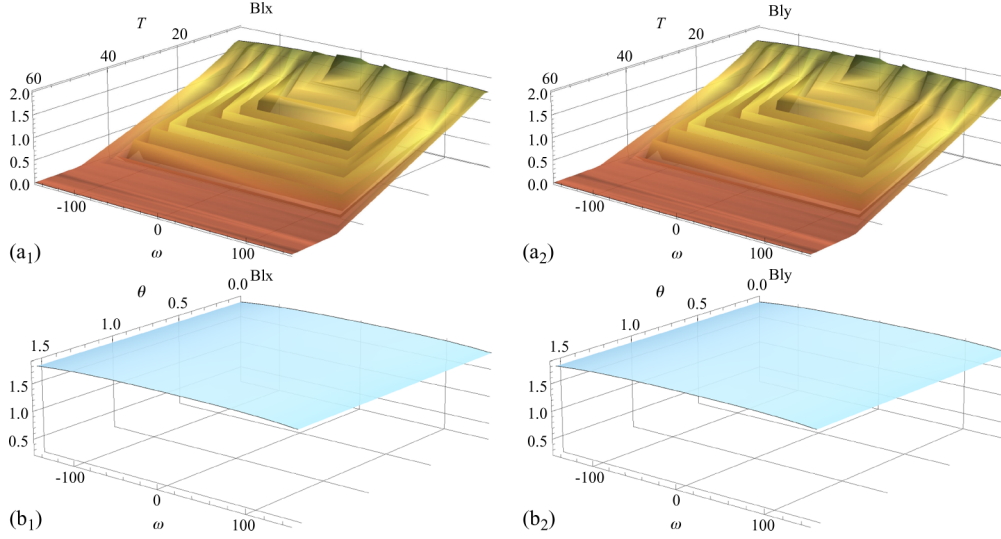$$A_{2y} = -\int \frac{d\mathbf{p}}{(2\pi)^2} \hat{D} \frac{\partial F_y}{\partial y_2}. \tag{B12d}$$

FIG. 7. (Color online) Typical solution for the pure QDW/SC solution, as a function of (ϵ_n, T) in (a_1) and (a_2) and as a function of (ϵ_n, θ) in (b_1) and (b_2). Values of the parameters are $g_1 = 20$, $g_2 = 30$, $v = 6$, $m_a = 0.1$, $\gamma = 3$, and $W = 2\pi$. The velocity angle is $\theta = 0.1$ for (a_1) and (a_2), whereas the temperature is $T = 1$ for (b_1) and (b_2). Note the very feeble dependence on the Fermi angle for this solution.

The expressions for the partial derivatives are given in Eq. (26). With this notation, the MFEs are written

$$\gamma_1^{-1} B_{1x} = -2T \sum_\epsilon b_{1x} A_{1x}, \tag{B13a}$$

$$\gamma_1^{-1} B_{1y} = -2T \sum_\epsilon b_{1y} A_{1y}, \tag{B13b}$$

$$\gamma_2^{-1} B_{2x} = -2T \sum_\epsilon b_{2x} A_{2x}, \tag{B13c}$$

$$\gamma_2^{-1} B_{2y} = -2T \sum_\epsilon b_{2y} A_{2y}. \tag{B13d}$$

We can finally write the result in the form of Eq. (25).

APPENDIX C: GAUSSIAN FLUCTUATIONS

Let us explicitly derive the stability condition for one order parameter b_x, b_y in the presence of Gaussian fluctuations. Noting that $x = b_x^2$ and $y = b_y^2$, we have

$$F = F_0 + F_x(x) + F_y(y). \tag{C1}$$

Using $B = B_0 + \delta B$ and $\overline{B} = \overline{B}_0 + \delta \overline{B}$ we get

$$F_0 = F_0^{(0)} + F_0^{(1)} + F_0^{(2)}, \tag{C2a}$$

$$F_0^{(1)} = J_{x-x'}^{-1}(\overline{B}_{x0}\delta B_x + B_{x0}\delta \overline{B}_x + \overline{B}_{y0}\delta B_{y0} + B_{y0}\delta \overline{B}_{y0}), \tag{C2b}$$

$$F_0^{(2)} = J_{x-x'}^{-1}(\delta \overline{B}_x \delta B_x + \delta \overline{B}_y \delta B_y). \tag{C2c}$$
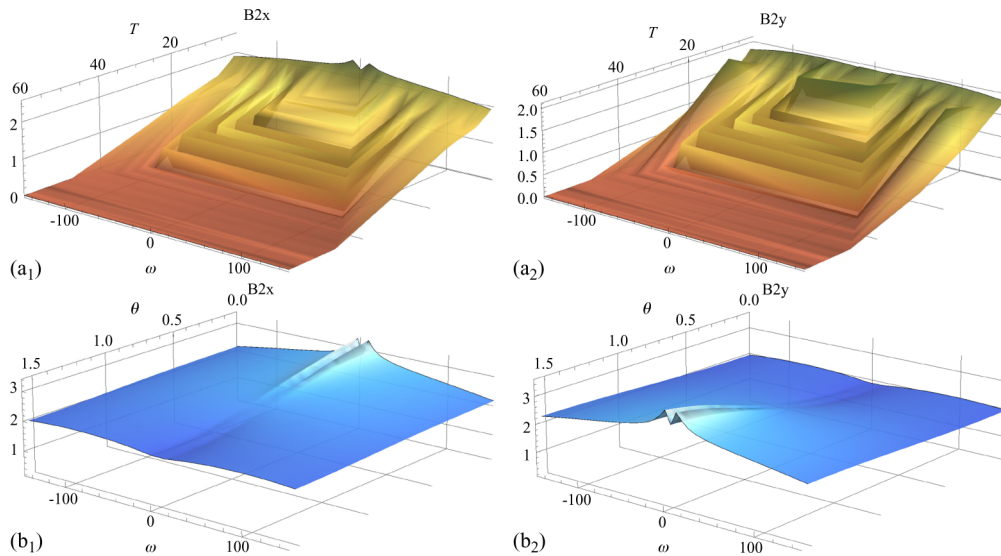

FIG. 8. (Color online) Typical solution for the pure CDW solution, as a function of (ϵ_n, T) for (a_1) and (a_2) and as a function of (ϵ_n, θ) for (b_1) and (b_2). Values of the parameters are $g_1 = 20$, $g_2 = 30$, $v = 6$, $m_a = 0.1$, $\gamma = 3$, and $W = 2\pi$. The velocity angle is $\theta = 0.1$ in (a_1) and (a_2), whereas the temperature is $T = 1$ in (b_1) and (b_2). Note that although the T dependence of the solution is different from that in Fig. 7, especially where the magnitude of the solution is concerned, its angular dependence is very similar to that depicted in Fig. 7.
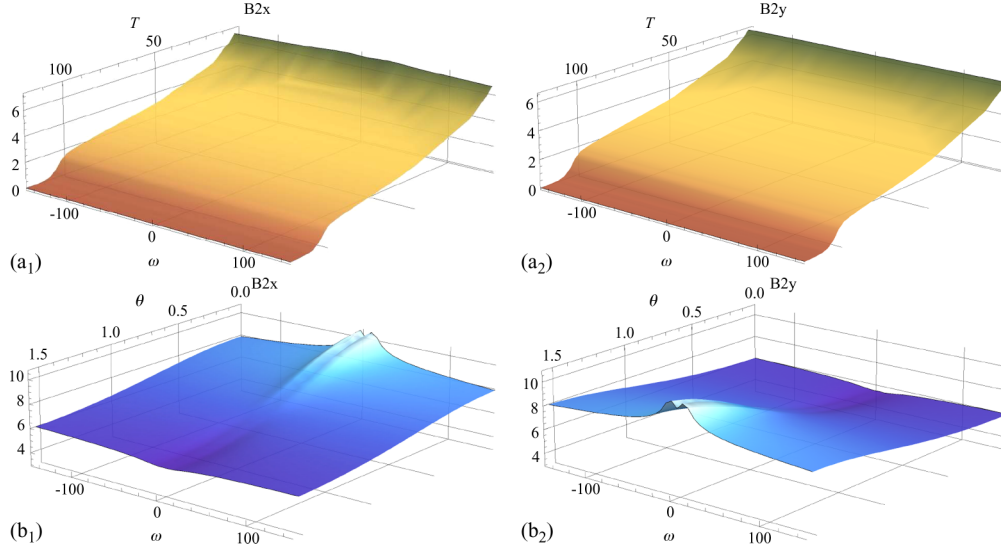
FIG. 9. (Color online) Typical solution for the pure CDW/PDW solution, as a function of (ϵ_n, T) in (a$_1$) and (a$_2$) and as a function of (ϵ_n, θ) in (b$_1$) and (b$_2$). Values of the parameters are $g_1 = 20$, $g_2 = 200$, $v = 6$, $m_a = 0.1$, $\gamma = 3$, and $W = 2\pi$. The velocity angle is $\theta = 0.1$ in (a$_1$) and (a$_2$), whereas the temperature is $T = 1$ in (b$_1$) and (b$_2$). Note the strong dependence on the Fermi angle for this solution.

From the mean-field relations $\overline{B}_{x0} = B_{y0}$ and $\overline{B}_{y0} = B_{x0}$ we obtain

$$F_0^{(1)} = J_{x-x'}^{-1}(B_{xo}\delta b_x + B_{y0}\delta b_y), \tag{C3a}$$

$$\delta b_x = \delta \overline{B}_x + \delta B_y, \tag{C3b}$$

$$\delta b_y = \delta \overline{B}_y + \delta B_x. \tag{C3c}$$

Now let us consider the second term in the free energy:

$$F_x^{(1)} = 2b_{x0}F_x'\delta b_x, \tag{C4a}$$

$$F_x^{(2)} = \left(F_x' + 2b_{x0}^2 F_x''\right)(\delta b_x)^2, \tag{C4b}$$

$$F_y^{(1)} = 2b_{y0}F_y'\delta b_y, \tag{C4c}$$

$$F_y^{(2)} = \left(F_y' + 2b_{y0}^2 F_y''\right)(\delta b_y)^2. \tag{C4d}$$

Hence we get, for the factors δA_i (notation: $x_1 = b_{1x}^2$, $x_2 = b_{2x}^2$, $y_1 = b_{1y}^2$, $y_2 = b_{2y}^2$),

$$\delta A_{1x} = 2\int \frac{d\mathbf{q}}{(2\pi)^2} D(\omega, \mathbf{q}) b_{1x}^2 \frac{\partial^2 F}{\partial x_1^2}, \tag{C5a}$$

$$\delta A_{2x} = 2\int \frac{d\mathbf{q}}{(2\pi)^2} D(\omega, \mathbf{q}) b_{2x}^2 \frac{\partial^2 F}{\partial x_2^2}, \tag{C5b}$$

$$\delta A_{1y} = 2\int \frac{d\mathbf{q}}{(2\pi)^2} D(\omega, \mathbf{q}) b_{1y}^2 \frac{\partial^2 F}{\partial y_1^2}, \tag{C5c}$$

$$\delta A_{2y} = 2\int \frac{d\mathbf{q}}{(2\pi)^2} D(\omega, \mathbf{q}) b_{2y}^2 \frac{\partial^2 F}{\partial y_2^2}, \tag{C5d}$$
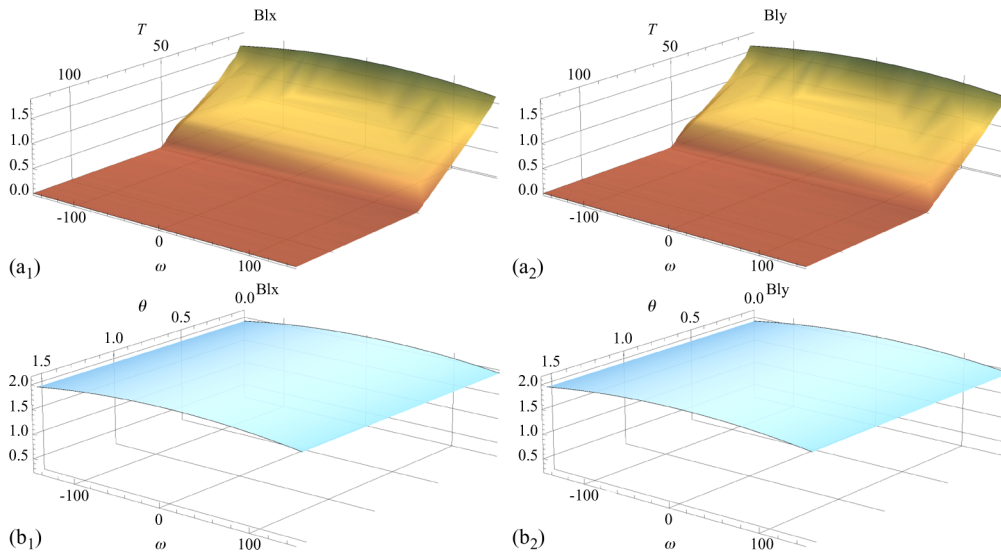

FIG. 10. (Color online) Typical solution for the pure QDW/SC solution, as a function of (ϵ_n, T) in (a$_1$) and (a$_2$) and as a function of (ϵ_n, θ) in (b$_1$) and (b$_2$). Values of the parameters are $g_1 = 20$, $g_2 = 200$, $v = 6$, $m_a = 0.1$, $\gamma = 3$, and $W = 2\pi$. The velocity angle is $\theta = 0.1$ in (a$_1$) and (a$_2$), whereas the temperature is $T = 1$ in (b$_1$) and (b$_2$). Note the striking similarities between this solution and the one in Fig. 7.
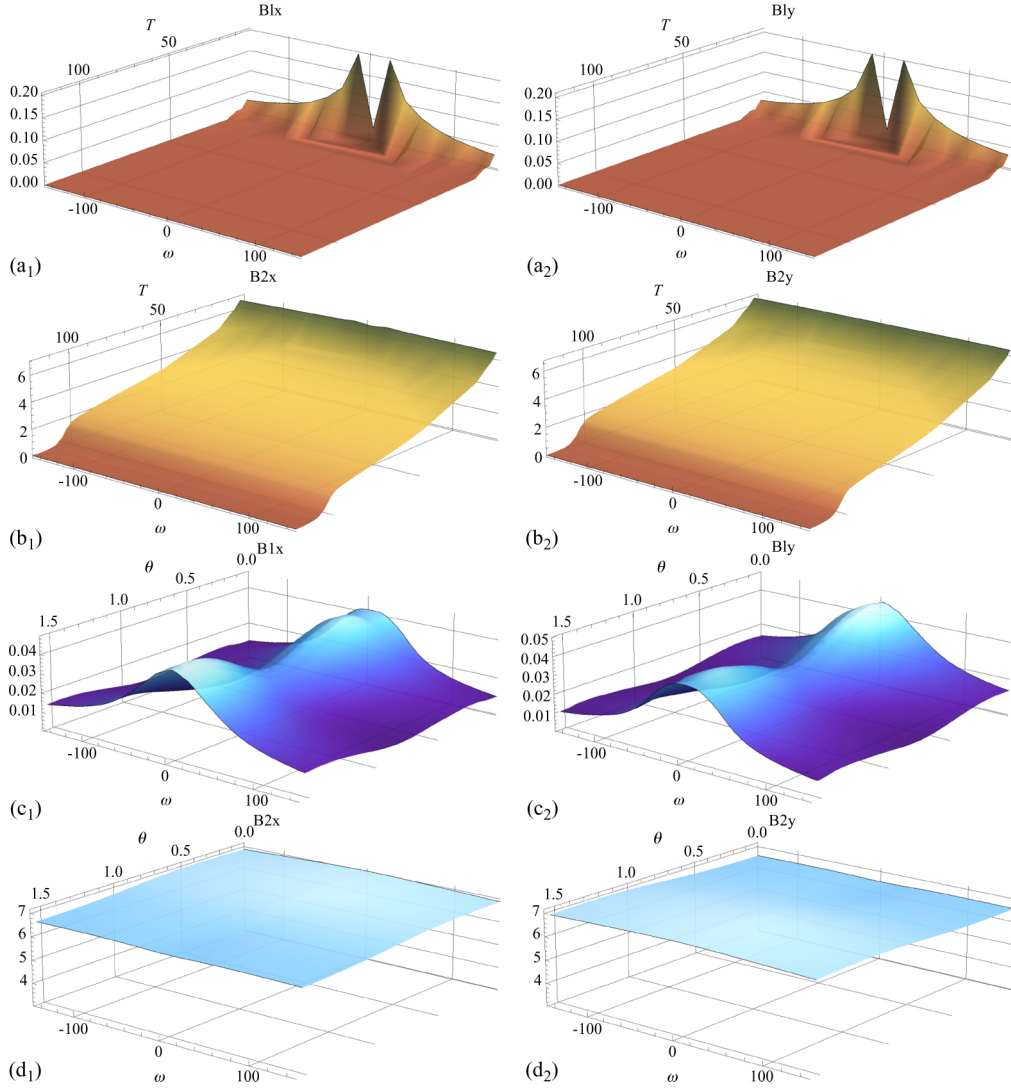
FIG. 11. (Color online) Typical solutions for the QDW/SC (B_{1x} and B_{1y}) and CDW (B_{2x} and B_{2y}) in the CE phase. Values of the parameters are $g_1 = 20$, $g_2 = 200$, $v = 6$, $m_a = 0.1$, $\gamma = 3$, and $W = 2\pi$. The velocity angle is $\theta = 0.1$ in (a_1), (a_2), (b_1), and (b_2), whereas the temperature is $T = 1$ in (c_1), (c_2), (d_1), and (d_2). Note the contrast with the CE solution in Fig. 2. Here the CDW/PDW component is one order of magnitude larger than the QDW/SC component and the θ dependence of the CDW/PDW component [(d_1) and (d_2)] is minimal compared to that of the QDW/SC component [(c_1) and (c_2)].
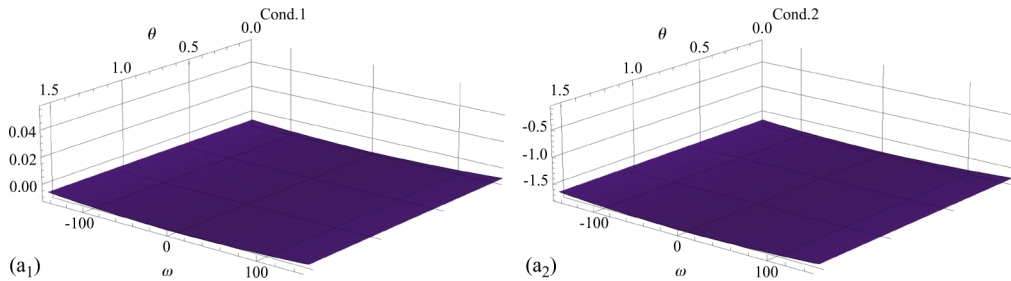

FIG. 12. (Color online) Stability conditions, (30), for the pure QDW/SC solution as a function of (ϵ_n, θ) at $T = 1$ K [(a_1) dir. B_1 and (a_2) dir. B_2]. Note that although the limit $J_2 \gg J_1$ is very unfavorable to this solution, it is still stable.
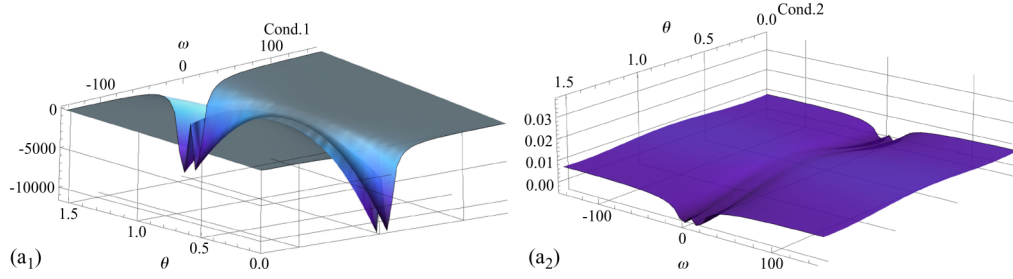
FIG. 13. (Color online) Stability conditions, (30), for the pure CDW/PDW solution as a function of (ϵ_n, θ) at $T = 1$ K [(a$_1$) dir B_1 and (a$_2$) dir B_2]. Note that although the limit $J_2 \gg J_1$ is energetically very favorable to this solution, there is a direction of instability (dir. B_1) at low temperatures, indicating instability towards the CE solution at lower temperatures.

with

$$\frac{\partial^2 F}{\partial x_1^2} = \frac{d_{\text{num}x1}}{d_{\text{den}x}}, \tag{C6a}$$

$$d_{\text{den}x} = \left(d_x^2 + 4vq_x vq_y \cos\theta \sin\theta d_x - 4b_{2x}^2 v^2 q_y^2 \sin^2\theta\right)^2, \tag{C6b}$$

$$d_{\text{num}x1} = d_x^2 + 4vq_x vq_y \cos\theta \sin\theta (d_x + 2vq_x vq_y \cos\theta \sin\theta) + 2b_{2x}^2 v^2 q_y^2 \sin^2\theta, \tag{C6c}$$

and

$$\frac{\partial^2 F}{\partial y_1^2} = \frac{d_{\text{num}y1}}{d_{\text{den}y}}, \tag{C7a}$$

$$d_{\text{den}y} = \left(d_y^2 + 4vq_x vq_y \cos\theta \sin\theta d_y - 4b_{2x}^2 v^2 q_y^2 \cos^2\theta\right)^2, \tag{C7b}$$

$$d_{\text{num}y1} = d_y^2 + 4vq_x vq_y \cos\theta \sin\theta (d_y + 2vq_x vq_y \cos\theta \sin\theta) + 2b_{2y}^2 v^2 q_y^2 \cos^2\theta, \tag{C7c}$$

and

$$\frac{\partial^2 F}{\partial x_2^2} = \frac{d_{\text{num}x2}}{d_{\text{den}x}}, \tag{C8a}$$

$$d_{\text{den}x} = \left(d_x^2 + 4vq_x vq_y \cos\theta \sin\theta d_x - 4b_{2x}^2 v^2 q_y^2 \sin^2\theta\right)^2, \tag{C8b}$$

$$d_{\text{num}x2} = d_x^2 + 4vq_x vq_y \cos\theta \sin\theta d_x - 4b_{2x}^2 v^2 q_y^2 \sin^2\theta \left(2b_{1x}^2 + 2\epsilon^2 + b_{2x}^2\right), \tag{C8c}$$

and

$$\frac{\partial^2 F}{\partial y_2^2} = \frac{d_{\text{num}y2}}{d_{\text{den}y}}, \tag{C9a}$$

$$d_{\text{den}y} = \left(d_y^2 + 4vq_x vq_y \cos\theta \sin\theta d_y - 4b_{2x}^2 v^2 q_y^2 \cos^2\theta\right)^2, \tag{C9b}$$

$$d_{\text{num}y2} = d_y^2 + 4vq_x vq_y \cos\theta \sin\theta d_y - 4b_{2y}^2 v^2 q_y^2 \cos^2\theta \left(2b_{1y}^2 + 2\epsilon^2 + b_{2y}^2\right). \tag{C9c}$$

APPENDIX D: STRUCTURE OF THE MEAN-FIELD SOLUTIONS

Let us give some more numerical solutions of the MFEs. In Fig. 2 are depicted the typical form of the QDW/SC and CDW/PDW components of the CE solution. Despite the CE solution, the MFEs, (25a)–(25d), admit two other solutions that we describe here.

The pure QDW/SC solution is depicted in Fig. 7. The most noticeable fact about this solution is the very feeble dependence on the Fermi velocity angle θ. This solution is very robust to changes in the shape of the Fermi surface at the hot spots and at the antinodes, characterized by $\theta = 0$ for flat portions of the Fermi surface at the antinodes and $\theta = \pi/4$ for the generic case. The pure QDW/SC solution is very similar to the observed PG of cuprate superconductors in that respect.

In contrast, the pure CDW/PDW solution depicted in Fig. 8 is much more dependent on the angle θ of the Fermi velocity at the antinodes.

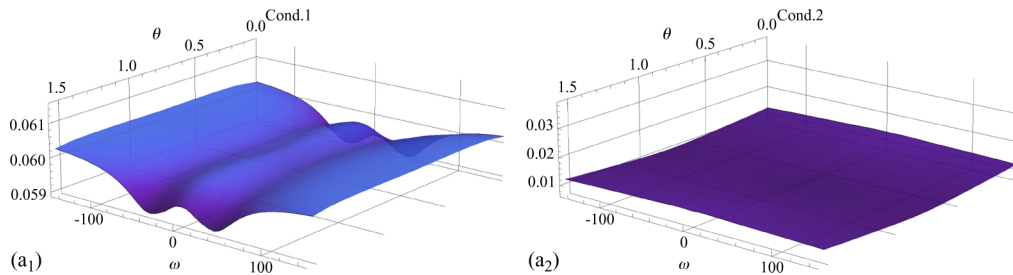FIG. 14. (Color online) Stability conditions, (30), for the pure CE solution as a function of (ϵ_n, θ) for $T = 1$ K. (a$_1$) Direction B_1 and (a$_2$) direction B_2. Note that the CE solution is stable in both directions at low temperatures.

APPENDIX E: EXTREME LIMIT WHERE $\gamma_1 \gg \gamma_0$

For completeness, let us discuss the extreme limit where $J_2 \gg J_1$ in Eqs. (25a)–(25d). Recently, an interesting work [54] has proposed the pure CDW solution as a candidate for the PG phase. This solution is preempted by the formation of a $q = 0$ bond state at the PG temperature T^*, which has the property of giving a nonzero Kerr signal [30]. It is interesting to see what happens within the study of CE when the quadratic coupling constant J_2 favoring the CDW order is pushed to a very high limit compared to J_1. This study is presented below for $J_2 = 10\, J_1$.

First, it is worth noting that the three solutions (pure CDW/PDW, pure QDW/SC, and the CE solution) are still present in the extreme limit where $J_2 \gg J_1$, which is extremely favorable to the pure CDW/PDW order. It happens that in this limit, the pure CDW/PDW solution becomes unstable towards the CE solution. Comparison of the free energies shows that the CE solution has a slightly lower energy than the pure CDW/PDW solution in this case, while the splitting is higher with the QDW/SC solution (Fig. 15).

1. MF solutions

We start with the pure CDW/PDW solution depicted in Fig. 9. One can observe the large magnitude of the pure CDW/PDW solution [Figs. 9(a_1) and 9(a_2)], whereas the θ dependence of the solution [Figs. 9(b_1) and 9(b_2)] has not changed compared to that in Fig. 8.

We turn now to the pure QDW/SC solution, which was introduced in Ref. [52] as a good candidate for the PG at T^*. Comparing Fig. 10 to Fig. 7, we see the similarity between the two solutions. This is to be expected since only the parameter J_2 has been increased between the two figures and the pure QDW/SC solution is insensitive to the value of J_2.

The CE solution is depicted in Fig. 11. The trend has been inverted compared to Fig. 2. Here the CDW/PDW component of the solution [Figs. 11(b_1) and 11(b_2)] is one order of magnitude larger than the pure QDW/SC component [Figs. 11(a_1) and 11(a_2)], in proportion to J_2/J_1. One can also note the pronounced θ dependence of the QDW/SC solution [Figs. 11(c_1) and 11(c_2)] compared to the CDW/PDW component [Figs. 11(d_1) and 11(d_2)]. This seems to confirm the intuition in Ref. [54] that it is possible to stabilize the CDW/PDW solution compared to the pure QDW/SC solution. The price to be paid, however, is to enforce $J_2 \gg J_1$ to such an extent that it seems rather artificial for high-T_c cuprates. Moreover, even when a giant CDW/PDW solution is stabilized,
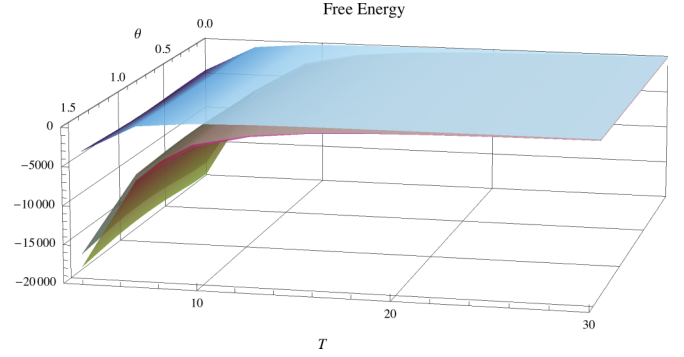

FIG. 15. (Color online) Free energy of the three mean-field solutions. Pure CDW/PDW (brown area), pure QDW/SC (dark-blue area), and CE (neon-colored areas). Values of the parameters are $g_1 = 20$, $g_2 = 200$, $v = 6$, $m_a = 0.1$, $\gamma = 3$, $W = 2\pi$, and $\theta = 0.1$.

we observed a re-entrance of the QDW/SC component at lower temperatures. The conclusion is that it is very difficult to get completely rid of the QDW/SC component.

2. Stability conditions

We now give the stability conditions for the various solution in the limit $J_2 \gg J_1$, in analogy with Fig. 4. The results of this investigation are quite unexpected. Although the limit $J_2 \gg J_1$ is extremely favorable to the pure CDW/PDW solution, we can see that at low temperatures (here the study is made at $T = 1$ K) this solution becomes unstable in the direction of the QDW/SC [dir. B_1 in our notation], indicating an instability towards CE at low temperatures. This observation corroborates the results in Appendix D, where it is concluded that it is very difficult to get completely rid of the QDW/SC solution. Note that the pure QDW/SC solution (Fig. 12) is now stable in one direction but becomes unstable in the direction of the CDW/PDW solution (Fig. 13), due to the favorable ratio $J_2/J_1 \gg 1$. Finally, the CE solution becomes stable in the two directions (Fig. 14).

3. Free energy

Finally, we turn to the comparison of the free energy for the three solutions in the limit $J_2 \gg J_1$. The result is shown in Fig. 15. By comparison with Fig. 5 we see that the energy of the pure QDW/SC solution is now higher than that of the pure CDW/PDW solution. The CE solution, however, is always the lowest energy one, although quite close in energy to the pure CDW/PDW solution. This supports our conclusion that the system is in general unstable towards the CE solution.

---

[1] J. E. Hoffman, E. W. Hudson, K. M. Lang, V. Madhavan, H. Eisaki, S. Uchida, and J. C. Davis, Science **295**, 466 (2002).

[2] T. Hanaguri, C. Lupien, Y. Kohsaka, D. H. Lee, M. Azuma, M. Takano, H. Takagi, and J. C. Davis, Nature **430**, 1001 (2004).

[3] K. McElroy, D.-H. Lee, J. E. Hoffman, K. M. Lang, J. Lee, E. W. Hudson, H. Eisaki, S. Uchida, and J. C. Davis, Phys. Rev. Lett. **94**, 197005 (2005).

[4] K. McElroy, G.-H. Gweon, S. Y. Zhou, J. Graf, S. Uchida, H. Eisaki, H. Takagi, T. Sasagawa, D.-H. Lee, and A. Lanzara, Phys. Rev. Lett. **96**, 067005 (2006).

[5] Y. Kohsaka, C. Taylor, K. Fujita, A. Schmidt, C. Lupien, T. Hanaguri, M. Azuma, M. Takano, H. Eisaki, H. Takagi, S. Uchida, and J. C. Davis, Science **315**, 1380 (2007).

[6] W. D. Wise, M. C. Boyer, K. Chatterjee, T. Kondo, T. Takeuchi, H. Ikuta, Y. Wang, and E. W. Hudson, Nat. Phys. **4**, 696 (2008).

 [7] Y. He, Y. Yin, M. Zech, A. Soumyanarayanan, M. M. Yee, T. Williams, M. C. Boyer, K. Chatterjee, W. D. Wise, I. Zeljkovic, T. Kondo, H. Ikuta, P. Mistark, R. S. Markiewicz, A. Bansil, S. Sachdev, E. W. Hudson, and J. E. Hoffman, Science **344**, 608 (2014).

 [8] E. H. da Silva Neto, P. Aynajian, A. Frano, R. Comin, E. Schierle, E. Weschke, A. Gyenis, J. Wen, J. Schneeloch, Z. Xu, S. Ono, G. Gu, M. Le Tacon, and A. Yazdani, Science **343**, 393 (2014).

 [9] N. Doiron-Leyraud, C. Proust, D. LeBoeuf, J. Levallois, J.-B. Bonnemaison, R. Liang, D. A. Bonn, W. N. Hardy, and L. Taillefer, Nature **447**, 565 (2007).

 [10] D. LeBoeuf, N. Doiron-Leyraud, J. Levallois, R. Daou, J. B. Bonnemaison, N. E. Hussey, L. Balicas, B. J. Ramshaw, R. Liang, D. A. Bonn, W. N. Hardy, S. Adachi, C. Proust, and L. Taillefer, Nature **450**, 533 (2007).

 [11] S. E. Sebastian, N. Harrison, M. M. Altarawneh, C. H. Mielke, R. Liang, D. A. Bonn, and G. G. Lonzarich, Proc. Natl. Acad. Sci. USA **107**, 6175 (2010).

 [12] F. Laliberté, J. Chang, N. Doiron-Leyraud, E. Hassinger, R. Daou, M. Rondeau, B. J. Ramshaw, R. Liang, D. A. Bonn, W. N. Hardy, S. Pyon, T. Takayama, H. Takagi, I. Sheikin, L. Malone, C. Proust, K. Behnia, and L. Taillefer, Nat. Commun. **2**, 432 (2011).

 [13] S. E. Sebastian, N. Harrison, R. Liang, D. A. Bonn, W. N. Hardy, C. H. Mielke, and G. G. Lonzarich, Phys. Rev. Lett. **108**, 196403 (2012).

 [14] T. Wu, H. Mayaffre, S. Krämer, M. Horvatic, C. Berthier, W. N. Hardy, R. Liang, D. A. Bonn, and M.-H. Julien, Nature **477**, 191 (2011).

 [15] T. Wu, H. Mayaffre, S. Krämer, M. Horvatić, C. Berthier, P. L. Kuhns, A. P. Reyes, R. Liang, W. N. Hardy, D. A. Bonn, and M.-H. Julien, Nat. Commun. **4**, 2113 (2013).

 [16] T. Wu, H. Mayaffre, S. Krämer, M. Horvatić, C. Berthier, W. N. Hardy, R. Liang, D. A. Bonn, and M.-H. Julien, arXiv:1404.1617 [cond-mat.supr-con].

 [17] D. LeBoeuf, S. Kramer, W. N. Hardy, R. Liang, D. A. Bonn, and C. Proust, Nat. Phys. **9**, 79 (2013).

 [18] A. Shekhter, B. J. Ramshaw, R. Liang, W. N. Hardy, D. A. Bonn, F. F. Balakirev, R. D. McDonald, J. B. Betts, S. C. Riggs, and A. Migliori, Nature **498**, 75 (2013).

 [19] M. Le Tacon, G. Ghiringhelli, J. Chaloupka, M. M. Sala, V. Hinkov, M. W. Haverkort, M. Minola, M. Bakr, K. J. Zhou, S. Blanco-Canosa, C. Monney, Y. T. Song, G. L. Sun, C. T. Lin, G. M. De Luca, M. Salluzzo, G. Khaliullin, T. Schmitt, L. Braicovich, and B. Keimer, Nat. Phys. **7**, 725 (2011).

 [20] J. Chang, E. Blackburn, A. T. Holmes, N. B. Christensen, J. Larsen, J. Mesot, R. Liang, D. A. Bonn, W. N. Hardy, A. Watenphul, M. v. Zimmermann, E. M. Forgan, and S. M. Hayden, Nat. Phys. **8**, 871 (2012).

 [21] G. Ghiringhelli, M. Le Tacon, M. Minola, S. Blanco-Canosa, C. Mazzoli, N. B. Brookes, G. M. De Luca, A. Frano, D. G. Hawthorn, F. He, T. Loew, M. M. Sala, D. C. Peets, M. Salluzzo, E. Schierle, R. Sutarto, G. A. Sawatzky, E. Weschke, B. Keimer, and L. Braicovich, Science **337**, 821 (2012).

 [22] E. Blackburn, J. Chang, A. H. Said, B. M. Leu, R. Liang, D. A. Bonn, W. N. Hardy, E. M. Forgan, and S. M. Hayden, Phys. Rev. B **88**, 054506 (2013).

 [23] S. Blanco-Canosa, A. Frano, T. Loew, Y. Lu, J. Porras, G. Ghiringhelli, M. Minola, C. Mazzoli, L. Braicovich,

 E. Schierle, E. Weschke, M. Le Tacon, and B. Keimer, Phys. Rev. Lett. **110**, 187001 (2013).

 [24] M. Le Tacon, A. Bosak, S. M. Souliou, G. Dellea, T. Loew, R. Heid, K.-P. Bohnen, G. Ghiringhelli, M. Krisch, and B. Keimer, Nat. Phys. **10**, 52 (2014).

 [25] S. Blanco-Canosa, A. Frano, E. Schierle, J. Porras, T. Loew, M. Minola, M. Bluschke, E. Weschke, B. Keimer, and M. Le Tacon, Phys. Rev. B **90**, 054513 (2014).

 [26] N. Harrison and S. E. Sebastian, Phys. Rev. Lett. **106**, 226402 (2011).

 [27] N. Harrison and S. E. Sebastian, New J. Phys. **16**, 063025 (2014).

 [28] I. M. Vishik, M. Hashimoto, R.-H. He, W.-S. Lee, F. Schmitt, D. Lu, R. G. Moore, C. Zhang, W. Meevasana, T. Sasagawa, S. Uchida, K. Fujita, S. Ishida, M. Ishikado, Y. Yoshida, H. Eisaki, Z. Hussain, T. P. Devereaux, and Z.-X. Shen, Proc. Natl. Acad. Sci. USA **109**, 18332 (2012).

 [29] R. Comin, A. Frano, M. M. Yee, Y. Yoshida, H. Eisaki, E. Schierle, E. Weschke, R. Sutarto, F. He, A. Soumyanarayanan, Y. He, M. Le Tacon, I. S. Elfimov, J. E. Hoffman, G. A. Sawatzky, B. Keimer, and A. Damascelli, Science **343**, 390 (2014).

 [30] J. Xia, E. Schemm, G. Deutscher, S. A. Kivelson, D. A. Bonn, W. N. Hardy, R. Liang, W. Siemons, G. Koster, M. M. Fejer, and A. Kapitulnik, Phys. Rev. Lett. **100**, 127002 (2008).

 [31] H. Alloul, T. Ohno, and P. Mendels, Phys. Rev. Lett. **63**, 1700 (1989).

 [32] W. W. Warren, R. E. Walstedt, G. F. Brennert, R. J. Cava, R. Tycko, R. F. Bell, and G. Dabbagh, Phys. Rev. Lett. **62**, 1193 (1989).

 [33] B. Fauqué, Y. Sidis, V. Hinkov, S. Pailhès, C. T. Lin, X. Chaud, and P. Bourges, Phys. Rev. Lett. **96**, 197001 (2006).

 [34] C. M. Varma, Phys. Rev. B **73**, 155113 (2006).

 [35] V. Balédent, D. Haug, Y. Sidis, V. Hinkov, C. T. Lin, and P. Bourges, Phys. Rev. B **83**, 104504 (2011).

 [36] P. Bourges and Y. Sidis, C.R. Phys. **12**, 461 (2011).

 [37] Y. Sidis and P. Bourges, J. Phys.: Conf. Ser. **449**, 012012 (2013).

 [38] G. Grissonnanche, O. Cyr-Choinière, F. Laliberté, S. Renéde Cotret, A. Juneau-Fecteau, S. Dufour-Beauséjour, M. È. Delage, D. LeBoeuf, J. Chang, B. J. Ramshaw, D. A. Bonn, W. N. Hardy, R. Liang, S. Adachi, N. E. Hussey, B. Vignolle, C. Proust, M. Sutherland, S. Krämer, J. H. Park, D. Graf, N. Doiron-Leyraud, and L. Taillefer, Nat. Commun. **5**, 3280 (2014).

 [39] H. Alloul, C.R. Phys. **15**, 519 (2014).

 [40] W. Tabis, Y. Li, M. Le Tacon, L. Braicovich, A. Kreyssig, M. Minola, G. Dellea, E. Weschke, M. J. Veit, M. Ramazanoglu, A. I. Goldman, T. Schmitt, G. Ghiringhelli, N. Barišić, M. K. Chan, C. J. Dorow, G. Yu, X. Zhao, B. Keimer, and M. Greven, arXiv:1404.7658 [cond-mat.supr-con].

 [41] S. Chakravarty, R. B. Laughlin, D. K. Morr, and C. Nayak, Phys. Rev. B **63**, 094503 (2001).

 [42] S. A. Kivelson, I. P. Bindloss, E. Fradkin, V. Oganesyan, J. M. Tranquada, A. Kapitulnik, and C. Howald, Rev. Mod. Phys. **75**, 1201 (2003).

 [43] E.-A. Kim, M. J. Lawler, P. Oreto, S. Sachdev, E. Fradkin, and S. A. Kivelson, Phys. Rev. B **77**, 184514 (2008).

 [44] A. Allais, J. Bauer, and S. Sachdev, Indian J. Phys. **88**, 905 (2014).

 [45] A. Allais, J. Bauer, and S. Sachdev, Phys. Rev. B **90**, 155114 (2014).

 [46] W. A. Atkinson, A. P. Kampf, and S. Bulut, arXiv:1404.1335 [cond-mat.supr-con].

[47] A. J. Millis and H. Monien, Phys. Rev. Lett. **70**, 2810 (1993).

[48] A. Abanov, A. V. Chubukov, and J. Schmalian, Adv. Phys. **52**, 119 (2003).

[49] A. Abanov and A. Chubukov, Phys. Rev. Lett. **93**, 255702 (2004).

[50] M. A. Metlitski and S. Sachdev, New J. Phys. **12**, 105007 (2010).

[51] M. A. Metlitski and S. Sachdev, Phys. Rev. B **82**, 075128 (2010).

[52] K. B. Efetov, H. Meier, and C. Pépin, Nat. Phys. **9**, 442 (2013).

[53] S. Sachdev and R. La Placa, Phys. Rev. Lett. **111**, 027202 (2013).

[54] Y. Wang and A. Chubukov, Phys. Rev. B **90**, 035149 (2014).

[55] M. Einenkel, H. Meier, C. Pépin, and K. B. Efetov, Phys. Rev. B **90**, 054511 (2014).

[56] L. E. Hayward, D. G. Hawthorn, R. G. Melko, and S. Sachdev, Science **343**, 1336 (2014).

[57] D. Chowdhury and S. Sachdev, Phys. Rev. B **90**, 134516 (2014).

[58] D. Chowdhury and S. Sachdev, arXiv:1409.5430 [cond-mat. str-el].

[59] R. Eder, W. Hanke, and S.-C. Zhang, Phys. Rev. B **57**, 13781 (1998).

[60] E. Demler, W. Hanke, and S. Zhang, Rev. Mod. Phys. **76**, 909 (2004).

[61] P. A. Lee, N. Nagaosa, and X.-G. Wen, Rev. Mod. Phys. **78**, 17 (2006).

[62] M. A. Metlitski and S. Sachdev, Phys. Rev. B **82**, 075127 (2010).

[63] H. Meier, M. Einenkel, C. Pépin, and K. B. Efetov, Phys. Rev. B **88**, 020506 (2013).

[64] H. Meier, C. Pépin, M. Einenkel, and K. B. Efetov, Phys. Rev. B **89**, 195115 (2014).

[65] K. Fujita, C. K. Kim, I. Lee, J. Lee, M. Hamidian, I. A. Firmo, S. Mukhopadhyay, H. Eisaki, S. Uchida, M. J. Lawler, E. A. Kim, and J. C. Davis, Science **344**, 612 (2014).

[66] V. S. de Carvalho and H. Freire, Ann. Phys. **348**, 32 (2014).

[67] A. Allais, D. Chowdhury, and S. Sachdev, arXiv:1406.0503 [cond-mat.str-el].

[68] P. A. Lee, Phys. Rev. X **4**, 031017 (2014).

[69] D. F. Agterberg, D. S. Melchert, and M. K. Kashyap, arXiv:1406.4959 [cond-mat.supr-con].

[70] E. Fradkin, S. A. Kivelson, and J. M. Tranquada, arXiv:1407.4480 [cond-mat.supr-con].